Transient JAK/STAT inhibition by ruxolitinib modulates malaria-specific CD4$^+$ T cell responses and enhances recall immunity in volunteers experimentally infected with *Plasmodium falciparum*.

Short: Host-directed modulation of CD4$^+$ T cell immunity.

Luzia Bukali[1], Damian Oyong[2], Fabian de Labastida Rivera[1], Jessica Engel[1], Rebecca Webster[1], Fiona Amante[1], Michael Leipold[3], Gerlinde Obermoser[3], Holden Maecker[3], James S. McCarthy[4], Bridget E Barber[1#], Michelle J. Boyle[2#] and Christian R. Engwerda[1#]

Author Affiliations:

1. QIMR Berghofer, Herston QLD, Australia
2. Burnet Institute, Melbourne, VIC, Australia
3. Stanford University, Stanford, CA, USA
4. Peter Doherty Institute for Infection and Immunity, Melbourne, Australia

# These authors contributed equally to this work

LB, DO FLR, JE and ML performed experiments and analysed data.

RW and FA managed the clinical trial and logistics of sample collection and processing.

HM, GO, JSM, BEB, MJB and CRE conceived and managed the project, analysed the data and wrote the manuscript.

Abstract

JAK/STAT signalling is a key regulator of $CD4^+$ T cell activation and function, influencing immune responses during infection. Ruxolitinib, a JAK1/2 inhibitor, transiently suppresses JAK/STAT signalling, but its impact on antigen-specific $CD4^+$ T cell responses in malaria is unknown. In this study, we assessed the effects of ruxolitinib on $CD4^+$ T cell cytokine signalling and immune responses using a controlled human malaria infection model. Whole blood was stimulated with IFNβ, IL-2, or PMA/Ionomycin, and phosphorylated STAT (pSTAT) expression was analysed. AIM assays and CyTOF were used to examine antigen-specific and memory $CD4^+$ T cell responses during primary and secondary infections. Ruxolitinib significantly reduced pSTAT1, pSTAT3, and pSTAT5 expression in $CD4^+$ T cells during treatment but did not impair antigen-specific responses. Instead, it enhanced recall immunity during secondary infection, particularly in AIM^+ T follicular helper (Tfh), T helper (Th)1, and type 1 regulatory (Tr1) cell subsets. Furthermore, increased frequencies of circulating Th1 and Tfh cells, but not Tr1 cells correlated with improved parasite control. These findings suggest that transient JAK inhibition modulates immune responses in a manner that could be leveraged as a host-directed therapy for malaria. Further research is needed to explore its potential applications in immune modulation for infectious diseases.

Introduction

Malaria remains a global health threat, with 263 million cases and 597,000 deaths reported by the WHO in 2023. Beyond its toll on health, malaria imposes socioeconomic burdens, particularly on disease endemic communities [1]. The recent WHO approval of two malaria vaccines, RTS,S and R21, offers progress, though limitations persist. These vaccines are only effective for a narrow age range (6 months to 5 years), with protection diminishing over time and efficacy falling short of the WHO's 75% target, especially in high-transmission areas [2]. Efforts to understand the reasons behind this poor vaccine performance indicate baseline immune characteristics play a key role [3, 4]. These characteristics not only shape responses to re-infection and vaccination but may also influence the efficacy of anti-parasitic drugs [5]. Hence, as we endeavour to combat malaria, acknowledging and addressing these immune nuances becomes imperative for developing effective intervention strategies for malaria control.

$CD4^+$ T cells play critical roles in coordinating immune responses and differentiating into functional subsets best suited to control pathogen growth, as well as controlling resulting inflammation [6]. For example, diseases caused by intracellular protozoan parasites like malaria, require the generation of IFNγ-producing, $Tbet^+$ $CD4^+$ (Th1) cells. These Th1 cells promote antigen processing and presentation by dendritic cells (DCs) and macrophages, and stimulate phagocytic cells to kill captured pathogens [7]. There is significant heterogeneity in the molecules expressed by Th1 cells, in part due to tissue-specific adaptions in response to infection-mediated changes to inflammation and metabolism [8]. This includes the emergence of counterbalancing cell subsets that regulate the inflammation caused by these cells [9, 10]. In regards to the latter, IL-10-producing Th1 cells (hereafter referred to as type 1 regulatory (Tr1) cells), develop as an important cell-autologous mechanism for dampening inflammation in African children living in malaria endemic areas [9, 10, 11, 12] and malaria-naïve volunteers participating in CHMI studies [13]. These Tr1 cells may also produce TGFβ and express a range of co-inhibitory receptor molecules to suppress inflammation, depending on the inflammatory context [14, 15]. However, although Tr1 cells protect tissue from inflammation [15, 16], they may also impair vaccine responses and responses to re-infection by suppressing anti-parasitic immunity [13, 17]. $CD4^+$ T follicular helper (Tfh) cells are another important $CD4^+$ T cell subset needed for the expansion of antigen-specific B cell populations

and the production of anti-parasitic antibody to clear parasitised red blood cells (pRBCs) during blood-stage malaria [18, 19]. Like Th1 cells, Tfh cells can also develop into different functional subsets, including those with Th1-, Th2- and Th17-like phenotypes that have pathogen-specific capacities to promote antibody production by germinal centre B cells [20, 21]. It has been shown that Th2-like circulating Tfh (cTfh) cells, but not other cTfh cell subsets, are associated with antibody development in volunteers participating in CHMI studies [22], as well as the presence of functional antibodies in children in a high malaria transmission area in Uganda [23]. The importance of Th2-like cTfh in generating effective anti-parasitic antibody responses has also been shown in human malaria vaccine trials [24, 25].

$CD4^+$ T cells are key mediators of immunological memory. Unlike naïve T cells, which require several days to initiate a response following infection, pathogen specific memory $CD4^+$ T cells respond much more quickly to reinfection [26]. Vaccines are designed to stimulate memory T and B cell development, but responses to vaccination can differ substantially between individuals. This can arise from established immunoregulatory networks [13, 27, 28, 29, 30]. In a pre-clinical malaria model, type I IFNs suppressed the development of anti-parasitic Tfh cell responses, thereby limiting parasite-specific antibody production [31]. We showed that type I IFNs also act on DCs to suppress the development of Th1 cells, while promoting *Il10* gene transcription in a model of experimental malaria [32]. We also demonstrated that type I IFNs suppressed antigen-specific IFNγ production, while promoting parasite-specific IL-10 production in volunteers participating in CHMI studies with *P. falciparum* [13]. Recently, we reported that the cytosolic DNA sensor stimulator of interferon genes (STING) was highly expressed by $CD4^+$ T cells and promoted autologous type I IFN-dependent development of Tr1 cells in volunteers infected with *Plasmodium falciparum* [33]. These findings led to the identification of a small molecule inhibitor (ruxolitinib) that blocks the type I IFN signaling pathway and acts synergistically with conventional anti-parasitic drug to improve parasite clearance and enhance anti-parasitic Th1 cell responses in mice and humans [33, 34]. We recently reported ruxolitinib was safe when administered to volunteers co-treated with the anti-malarial treatment artemether-lumefantrine [35], as well as volunteers participating in a CHMI study with *P. falciparum* 3D7 [36]. Here we report the impact of ruxolitinib as a host-directed treatment on $CD4^+$ T cells from volunteers in this Phase 1b clinical trial (ACTRN12621000866808).

Results

Effects of ruxolitinib on CD4$^+$ T Cell cytokine signalling pathways

We infected 20 malaria-naïve volunteers with *P. falciparum*-parasitised red blood cells (pRBCs). Participants were then randomised on day 8 or 9 post-infection to receive antimalarial treatment with artemether-lumefantrine with either ruxolitinb or placebo, each administered twice daily for 3 days. Fifteen of the participants were re-inoculated 3 months following the first infection [36]. We first examined the impact of ruxolitinib treatment on CD4$^+$ T cell cytokine signalling pathways by stimulating whole blood with IFNβ, IL-2, PMA/Ionomycin, or leaving it unstimulated (Fig. 1A). Clustering analysis of whole blood following CyTOF confirmed the identification of CD4$^+$ T cells and other immune cell subsets (Supplementary Fig. 1A). At day 0 (pre-inoculation), assessment of phosphorylated STAT (pSTAT) protein expression in CD4$^+$ T cells revealed that IFNβ stimulation increased pSTAT1 and pSTAT3 levels, while both IL-2 and IFNβ stimulation increased pSTAT5 expression, relative to baseline (unstimulated) conditions (Fig. 1B). Additionally, PMA/Ionomycin stimulation led to increased expression of phosphoproteins associated with alternative signalling pathways, including pCREB, pERK, and pS6 (Supplementary Fig. 1B). Based on these findings, subsequent analyses focused on key signalling molecules: pSTATs, pERK, pCREB, Ki67, and pS6 (mTOR pathway).

CD4$^+$ T cell subsets were identified using unsupervised clustering (Fig. 1C). *P. falciparum* infection influenced the expression of phosphoproteins, with enhanced pSTAT expression observed at the time of drug treatment (T), compared to time of infection (I) (Supplementary Fig. 1C). To assess the extent of the pSTAT response to ruxolitinib treatment, we measured fold changes in pSTAT1, pSTAT3, and pSTAT5 expression in total CD4$^+$ T cells and their subsets from before treatment (T) to midway through the 3-day regimen (T+1.5) under conditions of no *ex vivo* stimulation (Fig. 1D). While individual participants varied in the fold-change of pSTAT responses, treatment groups generally clustered together, with reduced pSTAT expression in the Rux group, compared to placebo (Fig. 1D). Notably, one participant (D722), who received only two doses of ruxolitinib, grouped with the placebo-treated participants rather than with other ruxolitinib-treated participants who had received at least three doses by T+1.5). Following IFNβ stimulation, pSTAT responses were again heterogeneous, yet participants largely grouped according to

treatment, with reduced pSTAT expression in the Rux group, compared to placebo (Fig. 1D) (Fig. 1E). The pSTAT3 response showed greater variability compared to pSTAT1 and pSTAT5, while low responders or the participantwith incomplete ruxolitinib treatment (D722) continued to cluster with the placebo group. Importantly, $CD4^+$ T cell subsets displayed similar response patterns to those observed in total $CD4^+$ T cells (Fig. 1D-E).

To further investigate the impact of ruxolitinib on alternative cytokine signalling pathways, we assessed pSTAT responses following IL-2 stimulation at the same timepoints. A reduction in pSTAT3 and pSTAT5 expression in the ruxolitinib-treated group compared to the placebo group was observed (Supplementary Fig. 2A). Conversely, phosphorylation of pERK and pCREB was highly variable, with minimal clustering according to treatment (Supplementary Fig. 2B). Together, these data indicate that ruxolitinib modulates STAT-dependent signalling in $CD4^+$ T cells, while its effects on alternative signalling pathways are more variable.

Ruxolitinib Inhibits JAK/STAT Signalling in $CD4^+$ T Cells but effects are transient

To quantify the effects of ruxolitinib on JAK/STAT signalling over time, we applied a linear mixed-effects model to compare pSTAT expression at the time of drug treatment (T), compared to subsequent time points across different stimulation conditions. The model outputs a coefficient that represents the direction and magnitude of change, with positive values indicating an increase and negative values indicating a decrease in phosphorylation relative to baseline. The placebo group serves as the reference for comparisons over time, while the interaction term (time*treatment) captures the effect of ruxolitinib treatment compared to placebo. In the placebo group, phosphorylation of STAT proteins increased significantly in all $CD4^+$ T cell subsets at T+1.5 in the absence of any direct *ex vivo* stimulation, followed by a reduction 5 days after treatment (T+5) (Fig. 2A). In contrast, ruxolitinib administration led to a marked, but transient reduction in pSTAT expression in all $CD4^+$ T cells under the same conditions at T+1.5 (Fig. 2B).

Following IFNβ stimulation, in the placebo group, pSTAT1 expression progressively increased from T to T+5 in most $CD4^+$ T cell subsets, whereas pSTAT5 expression transiently decreased from T to T+1.5 in activated (Act) and regulatory T (Treg) cells (Fig. 2C). In contrast, ruxolitinib treatment significantly reduced pSTAT1, pSTAT3, and pSTAT5 expression from T to T+1.5 in all $CD4^+$ T cell subsets, but expression levels returned to those of the placebo group by T+5 (Fig. 2D). A similar pattern was observed following IL-2 stimulation. In the

placebo group, pSTAT1 and pSTAT3 levels increased at T+1.5 before decreasing at T+5, while pSTAT5 expression remained relatively unchanged (Fig. 2E). However, in the ruxolitinib-treated group, pSTAT1, pSTAT3, and pSTAT5 levels in all $CD4^+$ T cell subsets were significantly reduced at T+1.5 compared to baseline (Fig. 2E). These findings confirm that ruxolitinib effectively suppresses JAK/STAT signalling, including both type I IFN and IL-2-mediated pathways.

Beyond STAT phosphorylation, ruxolitinib also exhibited off-target effects. Ki67, pCREB, pERK, and pS6 levels were all altered in response to treatment across different stimulation conditions (Supplementary Fig. 3), indicating broader immune modulation beyond the STAT pathway. Line plot representations of the linear mixed model results further illustrate the effects of ruxolitinib on pSTAT phosphorylation (Supplementary Fig. 4A-C). Specifically, in the placebo group, pSTAT expression increased markedly after treatment in stimulated and unstimulated conditions, peaking at T+1.5 (Supplementary Fig. 4A). In contrast, in all stimulation conditions, ruxolitinib significantly reduced pSTAT expression at T+1.5 compared to T (Supplementary Fig. 4A-C). Overall, these results confirm that ruxolitinib effectively inhibits JAK/STAT signalling in $CD4^+$ T cells, particularly at T+1.5. However, this inhibition is transient, as pSTAT expression returns to levels comparable to the placebo group by T+5. These findings highlight both the effectiveness and the temporal limitations of JAK inhibition in modulating immune signalling pathways.

Effects of ruxolitinib on antigen-specific $CD4^+$ T cell responses during primary and secondary infection

To investigate the impact of ruxolitinib on antigen-specific $CD4^+$ T cell responses, we utilized an Activation-Induced Marker (AIM) assay, with sample collection occurring at defined time points during both primary and secondary infection (Fig. 3A). The gating strategy used to identify AIM^+ $CD4^+$ T cells and their subsets is detailed in Supplementary Figure 5. In both treatment groups, only AIM^+ Tfh1 cell frequencies were significantly higher at re-infection compared to the primary infection, indicating an expansion of this subset only upon repeated exposure (Supplementary Fig. 6A). However, there was no evidence that this increase was impacted by ruxolitinib treatment (Supplementary Fig. 6B). This result contrasts with *ex vivo* assessment of $CD4^+$ T cell subset frequencies (without AIM assay), where, in both treatment groups, some $CD4^+$ T cell subsets were reduced at re-infection

compared to primary infection, while Th17 cell frequencies were notably higher at re-infection, suggesting a potential shift in immune dynamics upon repeated exposure to the parasite (Supplementary Fig. 6C). Importantly, ruxolitinib treatment during primary infection led to enhanced frequencies of activated Tfh1 and Th1 cells *ex vivo* at re-infection compared to their levels during the initial infection, further supporting the role of ruxolitinib in modulating long-term immune responses (Supplementary Fig. 6D).

In the placebo group, AIM$^+$ CD4$^+$ T cell frequencies significantly increased at T+7 and T+20 compared to baseline during primary infection. Similarly, during secondary infection, AIM$^+$ CD4$^+$ T cell populations were elevated 7 days after the start of drug treatment during re-infection (rT+7), relative to when drug treatment commenced (rT) (Fig. 3B). These findings suggest a robust antigen-specific CD4$^+$ T cell response following both primary and secondary infections. When comparing AIM$^+$ responses between the placebo and ruxolitinib-treated groups, there were no significant differences in frequencies of AIM$^+$ CD4$^+$ T cells during the primary infection, except for a reduction in AIM$^+$ Th2 cells at T+3 in the ruxolitinib group (Fig. 3C). However, during secondary infection, the ruxolitinib-treated group exhibited increased AIM$^+$ CD4$^+$ T cell frequencies at multiple time points, including rT+3, rT+7, and the end of study (EOS), compared to the placebo group. This suggests that ruxolitinib treatment during the primary infection may modulate the recall response upon secondary infection. Analysis of individual AIM$^+$ CD4$^+$ T cell subsets further highlighted these differences. Both the ruxolitinib and placebo groups displayed significant increases in total AIM$^+$ CD4$^+$ T cells (CD69$^+$ OX40$^+$) at T+7 and T+20 during primary infection. In the secondary infection, AIM$^+$ CD4$^+$ T cells were significantly elevated at rT+3 in the ruxolitinib-treated group relative to placebo, indicating an enhanced recall response (Fig. 3D). AIM$^+$ Tr1 cell frequencies increased at T+7 and T+20 in both groups during primary infection, with no treatment-related differences (Fig. 3E). However, in the secondary infection, these post-treatment increases in AIM$^+$ Tr1 cells were observed only in the ruxolitinib group, with AIM+ Tr1 cells higher at EOS in the ruxolitinib group relative to the placebo group. Similarly, frequency of AIM$^+$ Th1 cells also increased following treatment in both groups in primary infection, but significantly enhanced levels during secondary infection at rT+3 in the ruxolitinib-treated group, which declined by rT+7 (Fig. 3F). AIM$^+$ Tfh cell population frequencies increased at T+7 and T+20 during primary infection in both groups, with no significant treatment effects.

However, during secondary infection, AIM$^+$ Tfh frequencies were significantly elevated at all time points in the ruxolitinib group compared to rT (Fig. 3G). Importantly, AIM$^+$ Tfh cells were also significantly increased at rT+3 relative to the placebo group, suggesting that ruxolitinib administration during primary infection may enhance the Tfh recall response.

Further analysis of AIM$^+$ CD4$^+$ T cell subsets revealed additional differences in the ruxolitinib-treated group (Supplementary Fig. 7). Collectively, these findings indicate that while ruxolitinib does not significantly impair antigen-specific CD4$^+$ T cell responses during primary infection, it enhances the recall response upon secondary infection, particularly for AIM$^+$ Tr1, Th1, and Tfh cell populations.

Effects of ruxolitinib on Tr1 cell subsets during primary and secondary infection

To further investigate the impact of ruxolitinib on regulatory Tr1 cell populations, we applied unsupervised clustering to define Tr1 subsets and visualized these clusters using Uniform Manifold Approximation and Projection (UMAP) (Fig. 4A). A clustered heatmap revealed nine distinct Tr1 clusters based on their expression of activation and co-inhibitory markers (Fig. 4B). The gating strategy and analytical pipeline for identifying Tr1 cells are detailed in Supplementary Figure 8. Initial clustering analysis identified ten Tr1 clusters, which were further refined into nine clusters by merging highly similar populations (Supplementary Fig. 9A-C). Clusters were categorized based on their expression of co-inhibitory receptors, distinguishing between co-inhibitory receptor-rich and -poor subsets.

During primary infection, frequencies of the co-inhibitory receptor-rich and activated Tr1 clusters (C4, C7, and C8) were significantly increased at T+3 and T+7 in the placebo group (Fig. 4C). In the secondary infection, frequencies of C4 and C7 were similarly enhanced at rT+3, with C4 remaining elevated at rT+7. This pattern suggests that these Tr1 subsets are dynamically regulated in response to infection and may play a role in modulating immune responses upon re-exposure. Ruxolitinib treatment differentially affected Tr1 subsets. At T+3, the frequencies of co-inhibitory receptor-intermediate (C6) and -poor (C5) clusters were significantly enhanced in the ruxolitinib group, compared to placebo (Fig. 4D). However, the most co-inhibitory receptor-rich cluster (C4) was significantly reduced at T+3 in the ruxolitinib group compared to placebo. Additionally, the CD45RA$^+$ CCR7$^+$ cluster (C9) was reduced in the ruxolitinib group at both rT+3 and rT+7 compared to placebo, indicating that ruxolitinib may preferentially affect specific Tr1 subsets. C4, the most abundant co-

inhibitory receptor-rich Tr1 cluster, also expressed activation markers (CD38 and ICOS) and trafficking receptors (CXCR5 and CXCR3), suggesting a highly active phenotype (Fig. 4B). In the placebo group, this cluster was significantly increased at T+3, T+7, and EOS, whereas in the ruxolitinib group, C4 expansion was initially suppressed at T+3 but increased to placebo-comparable levels by T+7 and EOS (Fig. 4E). These findings indicate that ruxolitinib transiently suppresses this Tr1 cell subset, but its effects are not sustained. During secondary infection, C4 frequencies were significantly elevated at rT+3 and rT+7 in both the placebo and ruxolitinib groups, with no significant differences between treatment groups. This suggests that while ruxolitinib modulates Tr1 cell populations in the primary infection, its effects do not persist upon re-infection, allowing Tr1 cell subsets to expand similarly in both groups. Together, these findings demonstrate that ruxolitinib temporarily suppresses co-inhibitory receptor-rich Tr1 cell subsets during primary infection but does not impair their expansion during secondary infection. This transient effect may have implications for immune regulation and pathogen-specific tolerance in the context of JAK inhibition.

Effects of ruxolitinib on $CD4^+$ T cell subsets and their association with parasite control

To comprehensively assess the impact of ruxolitinib on $CD4^+$ T cell subset dynamics, we performed high-dimensional CyTOF analysis to define major immune populations within PBMCs (Supplementary Fig. 10A). $CD4^+$ T cells were further stratified using an over-clustering approach (k=60 FlowSOM clustering) to delineate 18 $CD4^+$ T cell subsets based on their chemokine receptor and activation marker expression (Supplementary Fig. 10B-C). In the placebo group, the frequencies of activated Th1 cells were significantly increased at T+3 and T+7, whereas activated Tfh cells were significantly reduced at T+7 and T+20 (Supplementary Fig. 10D). During secondary infection, multiple $CD4^+$ T cell subsets, particularly those expressing activation markers, were significantly elevated compared to the drug treatment time point (rT), suggesting a heightened recall response. Ruxolitinib treatment modulated $CD4^+$ T cell subset frequencies in both primary and secondary infections. At T+7, Tr1 and activated Tfh cell populations were significantly enriched in the ruxolitinib group compared to placebo (Supplementary Fig. 10E). During secondary infection, activated Tfh, Tfh1, Th1, and Tfh17 cell populations were all significantly increased in the ruxolitinib-treated group relative to placebo. A closer examination of activated Tfh cells revealed that their frequencies were significantly increased at T+7 in the ruxolitinib

group during primary infection, a trend that persisted through secondary infection, where they remained elevated at treatment following re-inoculation (rT), rT+7, and at EOS (Supplementary Fig. 10F). Similarly, activated Th1 cells peaked at T+7 in primary infection and at rT+3 during re-infection, suggesting a potential role in the development of memory responses. However, no significant differences were observed between treatment groups for this population (Supplementary Fig. 10G).

To assess whether ruxolitinib-induced changes in $CD4^+$ T cell subsets were linked to parasite control, we analysed the relationship between fold changes in $CD4^+$ T cell frequencies from rT to rT+3 and the parasite multiplication rate (PMR (48)) in re-infected participants (Fig. 5). This analysis included all eight participants from the ruxolitinib group, including D722 (who received only two doses) and D572 (who received three doses) during primary infection. In participants who received ruxolitinib, higher frequencies of both activated and non-activated Th1 cells were associated with a lower parasite multiplication rate, suggesting that these cells play a critical role in anti-parasitic immunity (Fig. 5A-B). Similarly, increased frequencies of non-activated Tfh cells were associated with reduced parasite multiplication rates in the ruxolitinib-treated group (Fig. 5C). Among the Tfh subsets, enhanced frequencies of Tfh17 cells showed the strongest association with reduced parasite multiplication rates (Fig. 5D), indicating a potentially protective function for this subset.

Discussion

Our findings demonstrate that in volunteers infected with *P. falciparum* and randomly assigned to receive the antimalarial artemether-lumefantrine with either ruxolitinib or a placebo, ruxolitinib effectively suppressed JAK/STAT signalling in CD4+ T cells. This was evidenced by a transient reduction in pSTAT1, pSTAT3, and pSTAT5 expression in response to malaria and cytokine stimulation. While this inhibition was pronounced during the drug treatment period, pSTAT expression returned to placebo-comparable levels two days after treatment ceased, highlighting the temporary nature of JAK inhibition. Importantly, ruxolitinib treatment did not significantly impair antigen-specific $CD4^+$ T cell responses during primary infection but was associated with enhanced recall responses upon secondary infection, particularly in AIM^+ Tfh1, Th1, and Tr1 cell populations. Additionally, ruxolitinib-induced changes in $CD4^+$ T cell subsets correlated with improved parasite control following re-infection, suggesting that modulation of these specific immune subsets may contribute to host defence. These findings provide novel insights into the immunomodulatory effects of ruxolitinib and its potential implications for host-directed therapies in infectious diseases.

Host-directed treatment is being tested in various infectious diseases [37]. For malaria, two broad approaches are considered: first, strategies to suppress acute inflammation associated with severe malaria syndromes [38, 39], and second, efforts to boost natural-, vaccine-, or anti-parasitic drug-mediated immunity [40]. Regarding the first approach, we reported that ruxolitinib attenuated the post-treatment increase in plasma levels of acute inflammatory markers, including C-reactive protein, alanine transaminase, and angiopoietin-2, in the same CHMI study described in this report [36]. Our demonstration that adjunctive ruxolitinib treatment enhances anti-parasitic Th1 and Tfh cell responses following re-infection provides reassurance that this drug does not compromise, and may even support, protective anti-parasitic immunity.

An important observation from our study was the large variation in response to ruxolitinib treatment between infected individuals. This variation has been reported in other clinical studies, including those investigating myelofibrosis [41], localized (skin) inflammation [42], and systemic inflammation [43]. While our study focused on $CD4^+$ T cell responses, we also observed variability in monocyte responses [36], suggesting that differences in immune modulation extended beyond the T cell compartment. This variability has implications for

future host-directed strategies, particularly if such approaches are to be deployed in mass drug administration campaigns or as adjunctive vaccination strategies. Identifying the underlying causes of this variation, whether genetic, environmental, or microbiome-related, will be critical to achieving greater consistency in responses.

One of the main goals of our host-directed strategy was to transiently limit the development of Tr1 cells in volunteers infected with *P. falciparum* following anti-parasitic drug treatment. We [14] and others [44] have previously reported that co-inhibitory receptor expression among Tr1 cells is highly variable, both in terms of receptor type and expression level. We found that the development of co-inhibitory receptor-rich Tr1 cells was most affected by ruxolitinib treatment. This was expected given the existence of an autologous, type I IFN-dependent pathway for Tr1 cell development, which regulates co-inhibitory receptor expression and IL-10 production [33]. Ruxolitinib's ability to target type I IFN signalling in children with interferonopathies [45] and in patients with dermatomyositis [46] supports our findings, showing a substantial impact on type I IFN-mediated Tr1 cell development. The transient nature of this effect further suggests that limiting Tr1 cell expansion does not increase the risk of excessive inflammation, supported by our clinical observations [36].

Despite the transient suppression of co-inhibitory receptor-rich Tr1 cell development following ruxolitinib treatment, there were minimal changes in other antigen-specific effector $CD4^+$ T cell subsets, such as Th1 and Tfh cells, after treatment during primary infection. One possible explanation is that ruxolitinib broadly affects multiple immune cell populations and effector functions, leading to counterbalancing pro- and anti-inflammatory effects, as reported here and in other studies [36]. Nevertheless, blockade of JAK1/2 signalling during initial infection shaped long-term immunity, as indicated by enhanced parasite-specific Tfh, Th1, and Tr1 cell responses following exposure to a second *P. falciparum* infection.

The increased Tr1 cell responses following secondary infection are likely linked to enhanced Th1 cell responses, given the close relationship between these subsets [15, 16]. Furthermore, the expansion of Tr1 cells during secondary infection did not appear to impair Th1 cell-mediated parasite control, as higher Th1 cell frequencies correlated with better parasite growth suppression. Similarly, increased Tfh cell frequencies were associated with improved parasite control following reinfection, supporting the critical role of these cells in generating

parasite-specific antibodies necessary for effective parasite clearance [22, 23, 40]. Notably, ruxolitinib treatment primarily expanded Tfh1 cells, a subset critical for antibody production in viral infections such as HIV [47], SARS-CoV-2 [48], and influenza [20]. In contrast, Tfh2 cells, which are thought to be important for antibody responses during malaria [22], were not significantly altered by ruxolitinib. The implications of this shift in Tfh subset dynamics remain unclear, but the overall positive correlation between Tfh frequencies and parasite control suggests that this balance may enhance protective immunity. Furthermore, a modest but significant improvement in parasite control during secondary infection, as indicated by reduced parasite multiplication rate, was observed regardless of ruxolitinib treatment [36].

Our findings have important implications for malaria elimination strategies. The ability of ruxolitinib to modulate $CD4^+$ T cell responses without impairing antigen-specific immunity suggests that transient JAK inhibition could enhance host immune control of *Plasmodium* infection. Enhancing recall immunity during secondary infection could be particularly relevant in endemic regions where repeated malaria exposure occurs, potentially improving naturally acquired immunity and reducing parasite burden over time. Additionally, the correlation between increased Th1 and Tfh cell frequencies with lower parasite multiplication rates suggests that immune modulation may help shape more effective, long-term protective immunity. Integrating host-directed therapies like ruxolitinib into malaria control programs could complement existing antimalarial strategies by improving immune responses to vaccines and drug treatments, ultimately reducing transmission and improving clinical outcomes. However, further studies are needed to evaluate the safety and feasibility of such interventions in different epidemiological settings and to determine their potential interactions with existing malaria vaccines and drug regimens.

Our study highlights the potential of JAK inhibition as an immunomodulatory strategy in malaria. While ruxolitinib effectively suppresses JAK/STAT signalling in $CD4^+$ T cells, its effects are transient, allowing for the recovery and modulation of immune responses over time. Importantly, ruxolitinib enhances antigen-specific recall responses upon secondary infection and is associated with improved parasite control. These findings underscore the need for further research into the use of JAK inhibitors as host-directed therapies for

malaria and other parasitic infections, with potential implications for immune modulation in infectious diseases more broadly.

Materials and Methods

Study ethics and approval

Samples in this study were part of a two-part phase Ib controlled human malaria infection clinical trial. The study is registered with the Australian New Zealand Clinical Trials Registry: ACTRN12621000866808.

Study cohort – The controlled human malarial infection study took place at the University of Sunshine Coast clinical trial sites in Brisbane, Australia. Study participants were healthy malaria-naïve adults aged 18 to 55 years who met the eligibility criteria (Table 1). Approval was obtained from the QIMRB Human Research Ethics Committee, ethics project number P1479.

Details of the study design are reported elsewhere [36]. In brief, in the first phase of the study, 20 participants were intravenously inoculated with 3D7 *P. falciparum*-infected RBCs. Blood parasitemia was monitored from day 4 post-infection using qPCR, and on day 8 or 9 participants were randomised to receive artemether-lumefantrine (AL) with either ruxolitinib or placebo. Participants and investigators were blinded to treatment allocation. 15 individuals returned for the second phase of the study and were re-inoculated with *P. falciparum*-infected RBCs 91 days post initial infection, and their blood parasitemia levels monitored as before. AL only was then administered once blood parasitemia levels exceeded 50,000 parasites/mL. One of the participants contracted SARS-CoV-2 during the re-infection period and was therefore excluded from subsequent analyses. Participants were monitored to ensure patient safety and parasite clearance up until six months post initial infection. Blood samples for immunological examination were collected on designated days throughout the trial.

Table 1: Participant information for the study cohorts.

Characteristic	All (n=20)	AL + Ruxolitinib (n=11)	AL + Placebo (n=9)
Sex, n (%)			
Male	11 (55%)	7 (64%)	4 (44%)
Age (years)			
Median (Range)	33 (18–55)	38 (21–55)	27 (18–41)
BMI (kg/m²)			
Median (Range)	25 (20–31)	26 (21–31)	25 (20–29)
Race, n (%)			
White	17 (85%)	8 (73%)	9 (100%)
Asian	1 (5%)	1 (9%)	0 (0%)
Other*	2 (10%)	2 (18%)	0 (0%)

Abbreviations: AL = artemether-lumefantrine; BMI = body mass index
*One participant reported their race as Colombian, and one as Iraqi.

Sample processing and PBMC Isolation

Whole blood from the study participants was collected into 10mL lithium heparin tubes for Ficoll-gradient separation at the designated time points. Briefly, the tubes were centrifuged at 2800 rpm (1578xg) for 10 minutes at RT with the acceleration and brake set to 6 (Eppendorf Centrifuge 5810R, Thermo Fisher Scientific). The following steps were carried out under sterile conditions. After centrifugation, the blood pellet was transferred into a 50mL Falcon tube and resuspended in 1X PBS (QIMR Berghofer) in a 1:1 ratio. The blood/PBS mixture was then layered onto 15mL of Ficoll-Paque PLUS (GE Healthcare). The Falcon tubes were then centrifuged at 1410rpm (400xg) for 20 minutes at RT with the acceleration on and the brake off. PBMCs were carefully collected from the buffy coat layer using a 1mL transfer pipette and transferred into a separate 50mL Falcon tube. The buffy coat was topped up to 50mL with 1X PBS and then centrifuged at 1500 rpm (453xg) for 10 minutes at RT with the acceleration and brake on. The supernatant was discarded and the pellet resuspended in 50mL of 1X PBS and washed again with the same settings for 5 minutes. The pellet was resuspended in 10mL of 1X PBS if the blood was obtained from 3 LiHep tubes and 20mL of 1X PBS if more than 3 LiHep tubes were used. 10µL of the cell solution was then mixed with CellDrop Acridine Orange/Propidium iodide (AO/PI) Viability Stain in a 1:1 ratio and loaded onto the counting chamber on the DeNovix Cell Drop FL (DeNovix) and the live cell counts recorded. PBMCs were stored in cryopreservation media

(90% (v/v) FBS, 10% (v/v) DMSO) at $^{-}$80°C before transfer to long-term cryogenic liquid nitrogen storage.

PBMC thaw

Cryovials of cryopreserved PBMCs were warmed in a 37°C water bath. The thawed PBMCs were then transferred into a 10 mL conical centrifuge tube containing 9mL sterile RPMI (Gibco, Life Technologies), 10% FBS (heat-inactivated) and 1µL Benzonase Nuclease (Sigma-Aldrich). Tubes were then centrifuged at 1,500 rpm (453xg) for 5 minutes with the acceleration and brake on (Eppendorf Centrifuge 5810R). PBMCs were resuspended in 1mL of 10% (v/v) FBS/RPMI. 10µL of the cell suspension was then mixed with 10µL of AO/PI in a 1:1 ratio and loaded onto the counting chamber on the DeNovix Cell Drop FL. The live cell count and percentage were recorded.

Thawing *P. falciparum* parasite for the AIM assay

Cryovials containing *P. falciparum* parasitised RBCs or un-parasitised RBCs (in-house laboratory stock) were thawed at RT. 100µL of Malaria Thaw Solution (3.5% (w/v) Sodium Chloride) was added dropwise for every 10µL of frozen RBC. The RBCs were allowed to rest for 2 minutes before being centrifuged at 2000rpm (425xg) for 2 minutes (Eppendorf Centrifuge 5430). The supernatant was discarded and 100µL of MTS:1X PBS (in a 1:1 ratio) was then added to the RBCs and the solution rested for 2 minutes. The cells were then centrifuged with the same settings as before and the supernatant was discarded. 1mL of 10% FBS/RPMI was added to the cell pellet before gently re-suspending the cells using a pipette. 10µL of the sample was then mixed with 10µL of Trypan blue viability dye (0.4% solution, Gibco). The cell mixture was loaded onto a microcuvette for counting on the Countess II Automated cell counter (Thermo Fisher Scientific). The cell counts were recorded and the cells were spun down in the centrifuge with the same settings as before. Finally, the supernatant was discarded and the cells were resuspended in 10% FBS/RPMI and the volume adjusted to a concentration of 1 x 10^6 pRBC or uRBC per 50µL.

Activation Induced Marker (AIM) assay and surface stain

Freshly thawed PBMCs were resuspended in 10% FBS (v/v)/ RPMI, transferred to a 96 well U-bottom plate and the concentration adjusted to 10x10^6 cells/mL in a volume of 100µL. 100µL of RPMI was added to each well and the cells were then rested for 2 hours at 37°C 5%

(v/v) CO_2. Following this, 50µL of 10% FBS/RPMI containing parasitised RBCs or un-parasitised RBCs was then added to each well and resuspended gently. The cells were incubated for a further 18 hours at 37°C with 5% CO_2. Following this, the cells were centrifuged at 1500rpm (453xg) for 5 minutes with the acceleration and brake on and resuspended by vortex at maximum speed. A solution containing the pre-stain antibodies listed in Table 2 and Human Fc block (1/30) in a total volume of 50µL 2% FBS/RPMI (cRPMI) was added to the cells before incubation at 37°C, 5% CO_2 for 45 minutes. After this, the cells were washed once with cRPMI. Viability stain was performed with Live/Dead Blue (Invitrogen, Thermo Fisher Scientific, Cat# L23015) diluted 1/1,000 in 1X PBS and incubated in the dark at RT for 15 minutes. The cells were subsequently washed twice with 2% FBS/PBS. 50µl of surface stain antibodies consisting of the antibodies listed in Table 2, plus Brilliant Stain Buffer (BD Biosciences, San Jose, CA, USA, 1/10) diluted in 2% FBS/PBS was added to each well. Cells were incubated in the dark at RT for 15 minutes. After this, the cells were washed twice with 2% FBS/PBS. The cells were resuspended in 200µL of BD Stabilizing fixative (diluted 1 in 3 in MilliQ water) and incubated in the dark at RT for 20 minutes. The cells were then washed twice and resuspended in 2% FBS/PBS before acquisition on a Cytek Aurora 5 using Spectroflo software. Flow cytometry results were then analysed on FlowJo version 10.9.0.

AIM analysis

$CD4^+$ T cell subsets were gated and identified according to Supplementary Figure 5. Activation induced markers CD69 and OX40 were used to identify antigen specific cell populations. Boolean gating was used to assess the frequencies of AIM^+ populations (Supplementary Figure 5). Background subtraction to account for "bystander" and non-specific activation in the AIM^+ $CD4^+$ T cell population was performed as follows:

$$pRBC\left(\frac{Cell\ Count}{CD4\ Count} * 100\right) - uRBC\left(\frac{Cell\ Count}{CD4\ Count} * 100\right)$$

Negative values as a result of background subtraction were set to zero. Resultant cell frequencies were then log10 transformed and used as the input in a linear mixed effects model.

Mass Cytometry and PBMC Phenotyping

Cryopreserved PBMCs collected during the clinical trial were sent to the Human Immune Monitoring Centre (HIMC, Palo Alto, California, U.S.A) at Stanford University for mass cytometry (CyTOF). Experimental procedures were performed at the HIMC according to their protocols [49]. Antibody cocktails were premixed and frozen in aliquots at -80°C to facilitate staining standardization and stability. Following mass cytometry PBMC staining with a 36-antibody immune-phenotyping panel (Table 3) [49], the raw FCS files were uploaded onto FlowJo software. Live intact cells were gated, then exported and loaded in R Studio as a single dataset, with the longitudinal data from both infections, periods and treatment groups combined. The Spectre package [50] in R Studio was used to perform the subsequent multi-dimensional analyses. An ArcSinh data transformation and a scaling co-factor of 5 was applied to all the samples. Samples were subsampled to a total of 1,000,000 cells total. Subsampling was performed randomly but with consistent randomness for reproducibility. FlowSOM clustering was performed by random subsampling 50,000 cells from the dataset. The cells were clustered according to their expression of all the cell markers used in the mass cytometry panel with a k-value of 15. The CyCombine package [51] was used to check for any batch effects amongst the 6 cohorts and 5 CyTOF batches in a healthy control sample run with each batch. The UMAP function was used for dimensionality reduction with the default Spectre parameters. Cells were clustered according to immune cell lineage markers and immune cell subsets classified according to their surface expression [52]. To illustrate, $CD4^+$ T cells were classified as $CD19^-$, $CD56^-$, $CD16^-$, $CD14^-$, $CD11c^-$, $CD3^+$ $CD4^+$.

$CD4^+$ T cell analysis in Spectre

The $CD4^+$ T cell dataset from the PBMC phenotyping analysis were concatenated and compiled into a single dataset regardless of treatment and time point. The cells were then clustered according to the expression of the T cell markers (CD45RA, CCR7, CXCR3, CXCR5, CD127, CD25, LAG3 and CD49b) using FlowSOM clustering with the default Spectre settings. As a results of suboptimal LAG3 staining, an over-clustering approach was used with a meta.k value of 60 in order to isolate cells expressing LAG3. The data was subsampled to 2,500 cells per sample and visualised using UMAP dimensionality reduction using the run.umap function default Spectre package settings. The 60 $CD4^+$ T clusters were annotated according to the expression of the chemokine and activation markers [52]. A heatmap was

created using the make.pheatmap function in Spectre, with coloring according to the MSI for each marker and hierarchical clustering of both the cell populations and the markers. Following the identification of the cell subsets, the create.sumtable function was used to generate a summary table of the frequencies of the cell subsets as a percent of the total $CD4^+$ T cell population. The cell frequencies were then input into a linear mixed effects model for analysis.

PBMC T cell and coinhibitory receptor stain

Freshly thawed PBMCs ($1x10^6$per well) were aliquoted into a V-bottom 96 well plate (Corning). Cells were spun down at 1700rpm (582xg) for 2 minutes with the brake and acceleration on and resuspended by vortex at maximum speed. The Pre-Stain antibodies listed in Table 4 and Human Fc block (Invitrogen, 1/30) in a total volume of 30µL 2% FBS/RPMI (cRPMI) was added to the cells. The cells were then incubated at 37°C, 5% CO2 for 1 hour. After the hour, 30µl of surface stain antibodies listed in Table 4 and Brilliant Stain Buffer (1/10) diluted in 2% FBS/PBS was added to the each well and incubated for a further 30 minutes. After incubation, the cells were washed twice with 1X PBS. Viability staining was performed by adding 30µL of Live/Dead Blue (Invitrogen) diluted 1/1000 in 1X PBS to each well and the plate incubated in the dark at RT for 15 minutes. After this, the cells were washed twice with 2% FBS/PBS prior to intracellular staining.

PBMC intracellular stain

For intracellular staining of PBMCs, cells were initially fixed using FoxP3 eBioscience fixative/permeabilisation buffer (prepared as a 1:4 dilution of the fixative agent to fixative diluent). The fixation process was carried out at 4°C in the dark for 30 minutes. Following fixation, the cells were washed twice with 1X FoxP3 eBioscience Permeabilisation buffer (prepared as a 1:10 dilution of permeabilisation concentrate and MilliQ water). 50µL of intracellular antibodies consisting of anti-Ki67 BUV395 (B56, 1/200, BD Biosciences, 564071), anti-NKG7 PE (2G9A10F5, 1/1000, Life Technologies) and anti-CTLA-4 BV786 (BNI3, 1/120, BD Biosciences, 563931) antibodies diluted in permeabilisation buffer (10X) was added to each well. Cells were incubated in the dark, at RT for 30 minutes. After incubation, the cells were washed twice with permeabilisation buffer. 1X BD stabilising fixative was added to the cells and the cells incubated in the dark, at RT for 10 minutes. The fixative agent was then washed off and the cells resuspended in 2% FBS/PBS and stored at 4°C until

acquisition on the Cytek Aurora 5 flow cytometer using Spectroflo software. Flow cytometry results were then analysed on FlowJo version 10.9.0.

Spectre Tr1 cell analysis

Following flow cytometry, dead cells and doublets were excluded and the $CD3^+$ $CD8^-$ $CD4^+$ T cells were gated in FlowJo (Supplementary Figure 8). The 3.0 FCS files containing the CD4 data were subsequently exported and input into R. Data was concatenated regardless of time point and treatment group and cyCombine batch alignment was performed on all markers to ensure no batch effects were present in the dataset. Existing batch effects were corrected using the default cyCombine correct.batch.effects function. Next, a gating strategy was implemented to identify the cell populations of interest according to the expression of T cell markers. To focus specifically on the Tr1 cells, Treg cells ($CD127^{low}$ $CD25^+$) were first identified and removed from the main $CD4^+$ T cell population. A density plot with all the non-Treg cells was then used to visualise and isolate the cells that were $LAG3^+$ and $CD49b^+$ (Supplementary Figure 8). These cells were combined into a single dataset.

The Tr1 cells were clustered according to the expression of the T cell markers (CD45RA, CCR7, CXCR3, CXCR5, CCR2, CCR5, TIM3, TIGIT, CD38, ICOS, CTLA-4, PD-1, Ki67 and CD161) using FlowSOM clustering with meta.k value of 10 and the default Spectre settings. The Spectre make.pheatmap function was used to create a heat map to visualise the expression of the markers on the 10 Tr1 clusters and the create.sumtable function used to determine the frequencies of the clusters as a percentage of all Tr1 cells. The Tr1 cells were down sampled to 2,500 cells per sample and dimensionality reduction performed using the run.umap function. Analyses to assess the frequency variations in Tr1 clusters with infection or infection and treatment were subsequently performed using a linear mixed effects model.

Whole blood stimulation to measure phosphorylated proteins

Whole blood was collected from study participants into Lithium Heparin tubes. 200µL from each sample was then transferred into 1.1mL appropriately labelled microtubes. Whole blood samples were collected from the participants in the clinical trial at day 0 (baseline), at pre-treatment on day 8/9, on the second day of treatment day 9/10 (T+1.5, halfway through

the treatment regimen) and day 13/14 (T+5, 5 days after the final treatment). Working solutions of human recombinant cytokines; 2µg/mL of IL-6 (eBioscience, Cat# BMS341), 20µg/mL IFNβ (Peprotech, ThermoFisher Scientific, Cat# 300-02BC-20), and 300µg/mL IL-2 (Miltenyi Biotec, Australia, Cat# 130-091-746), were prepared by adding the appropriate volume of PBS to the stock. A working solution of PMA (Phorbol 12-myristate 13-acetate (Sigma-Aldrich, Cat# P8139)) was prepared to a concentration of 1x105ng/mL and Ionomycin (Sigma-Aldrich, Cat# I0634) was taken directly from an in-house stock solution of 747µg/mL. The blood samples were then treated with the various stimulation conditions of 0.1µg/mL IL-6 or 1µg/mL IFNβ or 50ng/mL IL-2 or 50ng/mL PMA and 0.4855µg/mL Ionomycin, or left untreated. Samples were incubated for 15 minutes at RT, after which Proteomic stabilising solution (Prot1, Smart Tubes Inc. via ThermoFisher Scientific, Cat# FSHNC0618275) was added to each sample. The samples were vortexed and incubated for a further 10 minutes at RT. The samples were then transferred to long term storage at -80°C immediately after incubation. Cryopreserved samples were transported to the Stanford HIMC for mass cytometry.

Phosphorylated protein and cell subset analysis

This analysis was performed at the Burnet Institute (Melbourne, Australia) according to their established methods for cell analysis. Briefly, following whole blood mass cytometry with the phosphoCyTOF 36-antibody panel (Table 5) at the Stanford HIMC panel [49], the raw FCS files were uploaded into R Studio for analysis using the Spectre package. The data was combined into one dataset regardless of the time point, treatment or stimulation condition. The data was ArcSinh transformed and subsequently batch corrected using the cyCombine package. FlowSOM clustering was performed using the cell lineage markers in the panel, a meta.k value of 20 and the default Spectre settings on the run.flowSOM function. The data was subsampled to 5000 cell per sample and the run.umap function with default settings used to visualise the 20 FlowSOM clusters. A default clustered heatmap and expression plots showing the mean expression of the clustering markers was used to identify the $CD4^+$ T cells [52].

Spectre $CD4^+$ T cell phosphorylated protein analysis

The batch corrected $CD4^+$ T cell dataset was loaded into R Studio for analysis with Spectre using the analytical pipeline we had previously established. First, the FlowSOM clustering

with the markers CD45RA, CD27, CD38, HLA-DR, CD127 and CD25 and the default settings was used to sub cluster the $CD4^+$ T cells with a meta.k value of 15. The data was then subsampled to 5000 cells per participant and visualised using the run.umap function. A clustered heatmap and density plots showing the expression of the clustering markers were used to annotate the clusters. After identification of the $CD4^+$ T cells, the create.sumtable function was used to obtain the frequency of the cells as a percentage of the total $CD4^+$ T cells and the mean signal intensity (MSI) of the phosphorylated proteins on the cells for each stimulation condition. The $CD4^+$ T cell frequencies and MSI of the phosphorylated proteins was used as input into the linear mixed effects model.

Statistical analysis

Statistical analysis of the $CD4^+$ T cell, Tr1 cluster frequencies and the MSI of the phosphorylated proteins was performed using a linear mixed effects model. The analysis was performed in R using R Studio (v. 4.3.1) using the Linear and Nonlinear mixed effects model (nlme) package (v. 3.1-163) and the Fit linear mixed-effects models package lme4 (v.1.1-35-5). To adjust the datasets and allow for log10 transformation, the results were transformed by adding half of the lowest value to the zero values prior to the transformation. Data were run with the restricted (residual) maximum likelihood (REML) function to optimise for better estimation of the fixed effects and to moderate heteroscedasticity. In the case where random effect is singular, standard linear regression is calculated. Non-normal residues were addressed using residual bootstrapping with the boot (v. 1.3-30) and the lmeresampler packages (v. 0.2.4). Essentially, when performing the linear mixed effects model, the data was repeatedly sampled 5000 times for optimal results.

To avoid over-fitting the model, statistical comparisons were made between the inoculation time point and subsequent sample collection time points in the 1st and 2nd infection. Differences over the course of infection and between participants treated with ruxolitinib versus those treated with placebo were assessed using the linear mixed effects model, with time point and treatment being the fixed effects and participant ID being the random effect. Intercept of the model was calculated for the 2nd infection to examine differences between the treatment groups at re-inoculation time point.

$$linear\ mixed\ effect\ model = Response \sim 1 + fixed\ 1 * fixed\ 2 + (1|random\ 1)$$

To summarise the data, plots were generated using the output from the linear mixed effects model with the coefficient of change over time or the interaction term of time and treatment on the y-axis and the time point on the x-axis. Line plots with the log10 transformed percentages or expression values were created to show changes over the course of infection for both phases of the clinical study in comparison to the respective treatment time points. Average predicted values from the model was used to determine the overall value for each treatment group.

The parasite multiplication rate (PMR) per 48 hours was calculated using previously reported methods [53]. Correlation analysis between the PMR48 and cell subset data was made only with the significant ($p < 0.05$) cell populations of interest. Spearman's correlation test was used to determine the correlations between the PMR48 and the log2 transformed fold change of the $CD4^+$ T cell subset frequencies or MSI of phosphoproteins from rT to rT+3 days. All plots were made with the R package ggplot2 [54] or ggpubr (v 0.6.0) [55].

Acknowledgements

We thank staff from the University of Sunshine Coast Clinical Trials team, volunteers who participated in the study, staff at the Queensland Paediatric Infectious Diseases Laboratory for conducting the malaria PCR assays, and members of the Stanford Human Immune Monitoring Center for technical assistance.

Data availability

Phospho-CyTOF whole blood and PBMC immunophenotyping Cy-TOF data is publicly available: DOI 10.5281/zenodo.14872946 and DOI 10.5281/zenodo.14873240, respectively.

Funding

This study was funded by the Australian National Health and Medical Research Council (NHMRC); Ideas Grant to BEB and MJB (GNT2002957). BEB and JCM are supported by NHMRC Investigator Grants (2016792 and 2016396 respectively); MJB is supported by a Snow Medical Fellowship (2022/SF167) and CSL Centenary Fellowship. The QIMR Berghofer Clinical Malaria group receives core funding from Medicines for Malaria Venture (MMV) to support the conduct of malaria volunteer infection studies.

Work in the Stanford Human Immune Monitoring Center was supported by the Gates Foundation [INV-008378]. The conclusions and opinions expressed in this work are those of the author(s) alone and shall not be attributed to the Foundation. Under the grant conditions of the Foundation, a Creative Commons Attribution 4.0 License has already been assigned to the Author Accepted Manuscript version that might arise from this submission.

Table 2: Antigen-induced marker assay flow cytometry panel

Antibody	**Clone**	**Source**	**Catalogue Number**
Pre-Stain			
Brilliant Violet 421 anti-human LAG3	T47-530	BD Biosciences	565720
FITC anti-human CD49b	Y418	Invitrogen	11-0498-42
PerCP Cy5.5 anti-human CD197 (CCR7)	G043H7	Biolegend	353220
Surface Stain			
Alexa Fluor 700 anti-human CD161	HP-3G10	Biolegend	339942
APC anti-human OX40	ACT35	BD Biosciences	563473
Brilliant Ultra-Violet 563 anti-human CD45RA	HI100	BD Biosciences	565702
Brilliant Ultra-Violet 496 anti-human CD8	RPA-T8	BD Biosciences	612942
Brilliant Ultra-Violet 805 anti-human CD3	SK7	BD Biosciences	612893
Brilliant Ultra-Violet 737 anti-human CD69	FN50	BD Biosciences	612817
Brilliant Violet 510 anti-human CD14	M5E2	Biolegend	301842
Brilliant Violet 510 anti-human CD19	HIB19	Biolegend	302241
Brilliant Violet 605 anti-human CCR4	L291H4	Biolegend	359418
Brilliant Violet 605 anti-human CCR6	11A9	BD Biosciences	563922
Brilliant Violet 711 anti-human CXCR5	J252D4	Biolegend	356934
Brilliant Violet 785 anti-human CD4	OKT4	Biolegend	317442
PE anti-human CD25	BC96	Biolegend	302906
PE/Cyanine 7 anti-human PD1	EH12.1	BD Biosciences	561272
PE/Fire 700 anti-human CD25	M-A251	Biolegend	356146

Table 3: PBMC immunophenotyping CyTOF panel

	PBMC phenotyping			
Metal label	**Specificity**	**Clone**	**Supplier**	**Conjugated by**
113In	CD57	HCD57	BioLegend	HIMC
115In	live/dead			
141Pr	CCR6	G034E3	Standard BioTools	Standard BioTools
142Nd	CD19	SJ25C1	Southern BioTech	HIMC
143Nd	CD4	SK3	BioLegend	HIMC
144Nd	CD8	SK1	BioLegend	HIMC
145Nd	CD39	A1	BioLegend	HIMC
146Nd	IgD	IA6-2	BioLegend	HIMC
147Sm	CD85j	292319	R&D Systems	HIMC
148Nd	CD11c	Bu15	BioLegend	HIMC
149Sm	CD16	3G8	BioLegend	HIMC
150Nd	CD3	UCHT1	BD	HIMC
151Eu	CD38	HB-7	BD	HIMC
152Sm	CD27	L128	BD	HIMC
153Eu	CD21	Bu32	BioLegend	HIMC
154Sm	CD14	M5E2	BioLegend	HIMC
155Gd	Vd2 TCR	B6	BioLegend	HIMC
156Gd	CD94	HP-3D9	BD	HIMC
157Gd	CD86	IT2.2	BioLegend	HIMC
158Gd	CXCR5	RF8B2	BD	HIMC
159Tb	CXCR3	G025H7	BioLegend	HIMC
160Gd	CCR7	150503	R&D Systems	HIMC
162Dy	CD45RA	HI100	BioLegend	HIMC
164Dy	CD20	2H7	BioLegend	HIMC
165Ho	CD127	A019D5	BioLegend	HIMC
166Er	CD33	P67.8	BD	HIMC
167Er	LAG3	11C3C65	BioLegend	HIMC
168Er	CD49b	P1E6-C5	BioLegend	HIMC
169Tm	ICOS	DX29	BD	HIMC
170Er	CD161	DX12	BD	HIMC
171Yb	TCRgd	B1	BioLegend	HIMC
172Yb	PD-1	EH12.1	BD	HIMC
173Yb	CD123	9F5	BD	HIMC
174Yb	CD56	NCAM16.2	BD	HIMC
175Lu	HLA-DR	G46-6	BD	HIMC
176Yb	CD25	M-A251	BD	HIMC
209YBi	CD11b	ICRF44	Standard BioTools	Standard BioTools

Table 4: Tr1 coinhibitory marker flow cytometry panel

Antibody	**Clone**	**Source**	**Catalogue Number**
Pre-Stain			
Alexa Fluor 647 anti-human LAG3	NA	Biolegend	369304
Allophycocyanin (APC)-Cy7 anti-human CCR2	K036C2	Australian Bioresearch	357220
Brilliant Violet 650 anti-human CCR5	3A9	BD Biosciences	564999
PE Dazzle anti-human TIGIT	VSTM3	Biolegend	372716
Brilliant Violet 605 anti-human TIM3	NA	JOMAR LIFE RESEARCH	16-3109-85
Surface Stain			
Alexa Fluor 700 anti-human CD161	HP-3G10	Biolegend	339942
Brilliant Ultra-Violet 563 anti-human CD45RA	HI100	BD Biosciences	565702
Brilliant Ultra-Violet 737 anti-human CD4	SK3	BD Biosciences	564305
Brilliant Ultra-Violet 496 anti-human CD8	RPA-T8	BD Biosciences	612942
Brilliant Ultra-Violet 805 anti-human CD3	SK7	BD Biosciences	612893
Brilliant Violet 421 anti-human CXCR3	IC6/CXCR3	BD Biosciences	562558
Brilliant Violet 480 anti-human CD38	HIT2	BD Biosciences	566137
Brilliant Violet 510 anti-human CD14	M5E2	Biolegend	301842
Brilliant Violet 510 anti-human CD19	SJ25C1	Biolegend	363020
Brilliant Violet 570 anti-human CD127	A019D5	Biolegend	351308
Brilliant Violet 711 anti-human CXCR5	J252D4	Biolegend	356934
Brilliant Violet 750 anti-human ICOS	C398.4A	Biolegend	313558
FITC anti-human CD49b	Y418	Invitrogen	11-0498-42
PE/Cyanine 7 anti-human PD1	EH12.1	BD Biosciences	561272
PE/Fire 640 anti-human CD16	3G8	Biolegend	302068
PE/Fire 700 anti-human CD25	M-A251	Biolegend	356146
PerCP Cy5.5 anti-human CD197 (CCR7)	150503	BD Biosciences	561144
Intra-cellular Stain			
Brilliant Violet 750 anti-human CTLA-4	BNI3	BD Biosciences	563931
Brilliant Ultra-Violet 395 anti-human Ki67	B56	BD Biosciences	564071
PE anti-human NKG7	2G9A10F5	Beckman Coulter	IM3293

Table 5: Whole blood phosph-CyTOF panel

Phospho-CyTOF				
Metal label	**Specificity**	**Clone**	**Supplier**	**Cat#**
89Y	CD45	HI30	Standard BioTools	3089003B
141Pr	CD7	CD7-6B7	Biolegend	343111
142Nd	CD19	HIB19	Standard BioTools	3142001B
143Nd	CD45RA	HI100	Standard BioTools	3143006B
144Nd	pPLCg2	K86-689.37	Standard BioTools	3144015A
145Nd	CD4	RPA-T4	Standard BioTools	3145001B
146Nd	IgD	IA6-2	Standard BioTools	3146005B
147Sm	CD20	2H7	Standard BioTools	3147007B
148Nd	IgA	Polyclonal	Standard BioTools	3148007B
149Sm	CD25	2A3	Standard BioTools	3149010B
150Nd	pStat5	47	Standard BioTools	3150005A
151Eu	CD123	6H6	Standard BioTools	3151001B
152Sm	Akt	D9E	Standard BioTools	3152005A
153Eu	pStat1	4a	Standard BioTools	3153005A
154Sm	CD127	R34-34	Novus Biological	DDX0700P-100
155Gd	CD27	L128	Standard BioTools	3155001B
156Gd	pP38	D3F9	Standard BioTools	3156002A
157Gd	CD24	ML-5	Biolegend	311102
158Gd	pStat3	4	Standard BioTools	3158005A
159Tb	CD11c	Bu15	Standard BioTools	3159001B
160Gd	CD14	M5E2	Standard BioTools	3160001B
162Dy	CD66b	80H3	Standard BioTools	3162023B
163Dy	CD56	NCAM16.2	Standard BioTools	3163007B
164Dy	IkBalpha	L35A5	Standard BioTools	3164004A
165Ho	CD16	B73.1	Standard BioTools	3167001B
167Er	CD38	HIT2	Standard BioTools	3168002B
168Er	CD8	SK1	Standard BioTools	3169010B
169Tm	CD33	WM53	Standard BioTools	3170001B
170Er	CD3	UCHT1	Standard BioTools	3167001B
171Yb	pERK 1/2	D13.14.4E	Standard BioTools	3171010A
172Yb	Ki67	B56	Standard BioTools	3172024B
173Yb	CD21	Bu32	Biolegend	354902
174Yb	HLA-DR	L243	Standard BioTools	3174001B
175Lu	pS6	N7548	Standard BioTools	3175009A
176Yb	CREB	87G3	Standard BioTools	3176005A
209Bi	CD11b	ICRF44	Standard BioTools	3209003B

References

1. WHO. World malaria report 2024. Geneva: World Health Organization; 2024.

2. Olotu, A. *et al.* Seven-Year Efficacy of RTS,S/AS01 Malaria Vaccine among Young African Children. *N Engl J Med* **374**, 2519-2529 (2016).

3. Moncunill, G. *et al.* Transcriptional correlates of malaria in RTS,S/AS01-vaccinated African children: a matched case-control study. *Elife* **11** (2022).

4. Oyong, D.A. *et al.* Distinct immune responses associated with vaccination status and protection outcomes after malaria challenge. *PLoS Pathog* **19**, e1011051 (2023).

5. Rogerson, S.J., Wijesinghe, R.S. & Meshnick, S.R. Host immunity as a determinant of treatment outcome in Plasmodium falciparum malaria. *Lancet Infect Dis* **10**, 51-59 (2010).

6. Sallusto, F. Heterogeneity of human CD4+ T cells against microbes. *Annual review of immunology* **34**, 317-334 (2016).

7. Tubo, N.J. & Jenkins, M.K. CD4+ T Cells: guardians of the phagosome. *Clinical microbiology reviews* **27**, 200-213 (2014).

8. Tuzlak, S. *et al.* Repositioning TH cell polarization from single cytokines to complex help. *Nature immunology* **22**, 1210-1217 (2021).

9. Boyle, M.J. *et al.* The Development of Plasmodium falciparum-Specific IL10 CD4 T Cells and Protection from Malaria in Children in an Area of High Malaria Transmission. *Front Immunol* **8**, 1329 (2017).

10. Jagannathan, P. *et al.* IFNgamma/IL-10 co-producing cells dominate the CD4 response to malaria in highly exposed children. *PLoS Pathog* **10**, e1003864 (2014).

11. Boyle, M.J. *et al.* Effector Phenotype of Plasmodium falciparum-Specific CD4+ T Cells Is Influenced by Both Age and Transmission Intensity in Naturally Exposed Populations. *J Infect Dis* **212**, 416-425 (2015).

12. Walther, M. *et al.* Distinct roles for FOXP3 and FOXP3 CD4 T cells in regulating cellular immunity to uncomplicated and severe Plasmodium falciparum malaria. *PLoS Pathog* **5**, e1000364 (2009).

13. Montes de Oca, M. *et al.* Type I Interferons Regulate Immune Responses in Humans with Blood-Stage Plasmodium falciparum Infection. *Cell Rep* **17**, 399-412 (2016).

14. Edwards, C.L. *et al.* IL-10-producing Th1 cells possess a distinct molecular signature in malaria. *The Journal of clinical investigation* **133** (2023).

15. Roncarolo, M.G., Gregori, S., Bacchetta, R., Battaglia, M. & Gagliani, N. The Biology of T Regulatory Type 1 Cells and Their Therapeutic Application in Immune-Mediated Diseases. *Immunity* **49**, 1004-1019 (2018).

16. Roncarolo, M.G., Gregori, S., Bacchetta, R. & Battaglia, M. Tr1 cells and the counter-regulation of immunity: natural mechanisms and therapeutic applications. *Current topics in microbiology and immunology* **380**, 39-68 (2014).

17. Montes de Oca, M. *et al.* Blimp-1-Dependent IL-10 Production by Tr1 Cells Regulates TNF-Mediated Tissue Pathology. *PLoS Pathog* **12**, e1005398 (2016).

18. Obeng-Adjei, N. *et al.* Circulating Th1-Cell-type Tfh Cells that Exhibit Impaired B Cell Help Are Preferentially Activated during Acute Malaria in Children. *Cell Rep* **13**, 425-439 (2015).

19. Ryg-Cornejo, V. *et al.* Severe Malaria Infections Impair Germinal Center Responses by Inhibiting T Follicular Helper Cell Differentiation. *Cell Rep* **14**, 68-81 (2016).

20. Bentebibel, S.E. *et al.* Induction of ICOS+CXCR3+CXCR5+ TH cells correlates with antibody responses to influenza vaccination. *Sci Transl Med* **5**, 176ra132 (2013).

21. Morita, R. *et al.* Human blood CXCR5(+)CD4(+) T cells are counterparts of T follicular cells and contain specific subsets that differentially support antibody secretion. *Immunity* **34**, 108-121 (2011).

22. Chan, J.A. *et al.* Th2-like T Follicular Helper Cells Promote Functional Antibody Production during Plasmodium falciparum Infection. *Cell Rep Med* **1**, 100157 (2020).

23. Chan, J.A. *et al.* Age-dependent changes in circulating Tfh cells influence development of functional malaria antibodies in children. *Nat Commun* **13**, 4159 (2022).

24. Bowyer, G. *et al.* CXCR3(+) T Follicular Helper Cells Induced by Co-Administration of RTS,S/AS01B and Viral-Vectored Vaccines Are Associated With Reduced Immunogenicity and Efficacy Against Malaria. *Front Immunol* **9**, 1660 (2018).

25. Nielsen, C.M. *et al.* Protein/AS01(B) vaccination elicits stronger, more Th2-skewed antigen-specific human T follicular helper cell responses than heterologous viral vectors. *Cell Rep Med* **2**, 100207 (2021).

26. Kunzli, M. & Masopust, D. CD4(+) T cell memory. *Nature immunology* **24**, 903-914 (2023).

27. Butler, N.S. *et al.* Therapeutic blockade of PD-L1 and LAG-3 rapidly clears established blood-stage Plasmodium infection. *Nature immunology* **13**, 188-195 (2011).

28. Edwards, C.L. *et al.* Early Changes in CD4+ T-Cell Activation During Blood-Stage Plasmodium falciparum Infection. *J Infect Dis* **218**, 1119-1129 (2018).

29. Montes de Oca, M., Good, M.F., McCarthy, J.S. & Engwerda, C.R. The Impact of Established Immunoregulatory Networks on Vaccine Efficacy and the Development of Immunity to Malaria. *J Immunol* **197**, 4518-4526 (2016).

30. Nahrendorf, W., Ivens, A. & Spence, P.J. Inducible mechanisms of disease tolerance provide an alternative strategy of acquired immunity to malaria. *Elife* **10** (2021).

31. Zander, R.A. *et al.* Type I Interferons Induce T Regulatory 1 Responses and Restrict Humoral Immunity during Experimental Malaria. *PLoS Pathog* **12**, e1005945 (2016).

32. Haque, A. *et al.* Type I IFN signaling in CD8- DCs impairs Th1-dependent malaria immunity. *The Journal of clinical investigation* **124**, 2483-2496 (2014).

33. Wang, Y. *et al.* STING activation promotes autologous type I interferon-dependent development of type 1 regulatory T cells during malaria. *The Journal of clinical investigation* **133** (2023).

34. Kumar, R. *et al.* Type I Interferons Suppress Anti-parasitic Immunity and Can Be Targeted to Improve Treatment of Visceral Leishmaniasis. *Cell Rep* **30**, 2512-2525 e2519 (2020).

35. Chughlay, M.F. *et al.* Safety, Tolerability, Pharmacokinetics, and Pharmacodynamics of Coadministered Ruxolitinib and Artemether-Lumefantrine in Healthy Adults. *Antimicrob Agents Chemother* **66**, e0158421 (2022).

36. Rebecca Webster, D.A.O., Azrin N. Abd-Rahman, Adam J. Potter, Reena Mukhiya, Nischal Sahai, Indika Leelasena, Eniko Ujvary, Sue Mathison, Dean W. Andrew, Luzia Bukali, Fabian de Labastida Rivera, Jessica Engel, Megan S.F. Soon, Teija Frame, Julianne Hamelink, Mayimuna Nalubega, Nicholas L. Dooley, Jessica R. Loughland, Tran Nguyen, Yael Rosenberg-Hasson, Sofia Maysel-Auslender, Natalia Sigal, Kira Foygel, Jeremy Gower, Jenny Peters, Ria Woo, Fiona Amante, Timothy N.C. Wells, Stephan Chalon, Joerg J. Moehrle, James S. McCarthy, Geoffrey W. Birrell, Michael D. Edstein, Michael Leipold, Gerlinde Obermoser, Holden Maecker, Christian R. Engwerda, Bridget E Barber, Michelle J. Boyle. Adjunctive ruxolitinib attenuates inflammation and enhances antiparasitic immunity in human volunteers experimentally infected with Plasmodium falciparum. *MedRxiv* (2025).

37. Zumla, A. *et al.* Host-directed therapies for infectious diseases: current status, recent progress, and future prospects. *Lancet Infect Dis* **16**, e47-63 (2016).

38. Adderley, J. & Grau, G.E. Host-directed therapies for malaria: possible applications and lessons from other indications. *Curr Opin Microbiol* **71**, 102228 (2023).

39. Wassmer, S.C., de Koning-Ward, T.F., Grau, G.E.R. & Pai, S. Unravelling mysteries at the perivascular space: a new rationale for cerebral malaria pathogenesis. *Trends Parasitol* **40**, 28-44 (2024).

40. Boyle, M.J., Engwerda, C.R. & Jagannathan, P. The impact of Plasmodium-driven immunoregulatory networks on immunity to malaria. *Nat Rev Immunol* (2024).

41. Mascarenhas, J. *et al.* Defining ruxolitinib failure and transition to next-line therapy for patients with myelofibrosis: a modified Delphi panel consensus study. *Future Oncol* **19**, 763-773 (2023).

42. Schell, S.L. *et al.* Pilot study of topical ruxolitinib demonstrates efficacy and blunting of heterogeneous inflammatory processes in mild hidradenitis suppurativa. *Br J Dermatol* (2024).

43. Zhang, Q. *et al.* A study of ruxolitinib response-based stratified treatment for pediatric hemophagocytic lymphohistiocytosis. *Blood* **139**, 3493-3504 (2022).

44. Brockmann, L. *et al.* Molecular and functional heterogeneity of IL-10-producing CD4(+) T cells. *Nat Commun* **9**, 5457 (2018).

45. Fremond, M.L. *et al.* Efficacy of the Janus kinase 1/2 inhibitor ruxolitinib in the treatment of vasculopathy associated with TMEM173-activating mutations in 3 children. *J Allergy Clin Immunol* **138**, 1752-1755 (2016).

46. Ladislau, L. *et al.* JAK inhibitor improves type I interferon induced damage: proof of concept in dermatomyositis. *Brain* **141**, 1609-1621 (2018).

47. Baiyegunhi, O. *et al.* Frequencies of Circulating Th1-Biased T Follicular Helper Cells in Acute HIV-1 Infection Correlate with the Development of HIV-Specific Antibody Responses and Lower Set Point Viral Load. *J Virol* **92** (2018).

48. Gong, F. *et al.* Peripheral CD4+ T cell subsets and antibody response in COVID-19 convalescent individuals. *The Journal of clinical investigation* **130**, 6588-6599 (2020).

49. Maecker, H.T., McCoy, J.P. & Nussenblatt, R. Standardizing immunophenotyping for the Human Immunology Project. *Nat Rev Immunol* **12**, 191-200 (2012).

50. Ashhurst, T.M. *et al.* Integration, exploration, and analysis of high-dimensional single-cell cytometry data using Spectre. *Cytometry A* **101**, 237-253 (2022).

51. Pedersen, C.B. *et al.* cyCombine allows for robust integration of single-cell cytometry datasets within and across technologies. *Nature Communications* **13**, 1698 (2022).

52. Jalali, S. *et al.* A high-dimensional cytometry atlas of peripheral blood over the human life span. *Immunology & Cell Biology* **100**, 805-821 (2022).

53. Wockner, L.F. *et al.* Growth Rate of *Plasmodium falciparum*: Analysis of Parasite Growth Data From Malaria Volunteer Infection Studies. *The Journal of Infectious Diseases* **221**, 963-972 (2020).

54. Wilkinson, L. ggplot2: elegant graphics for data analysis by WICKHAM, H. Oxford University Press; 2011.

55. Kassambara, A. ggpubr:'ggplot2'based publication ready plots. *R package version*, 2 (2018).

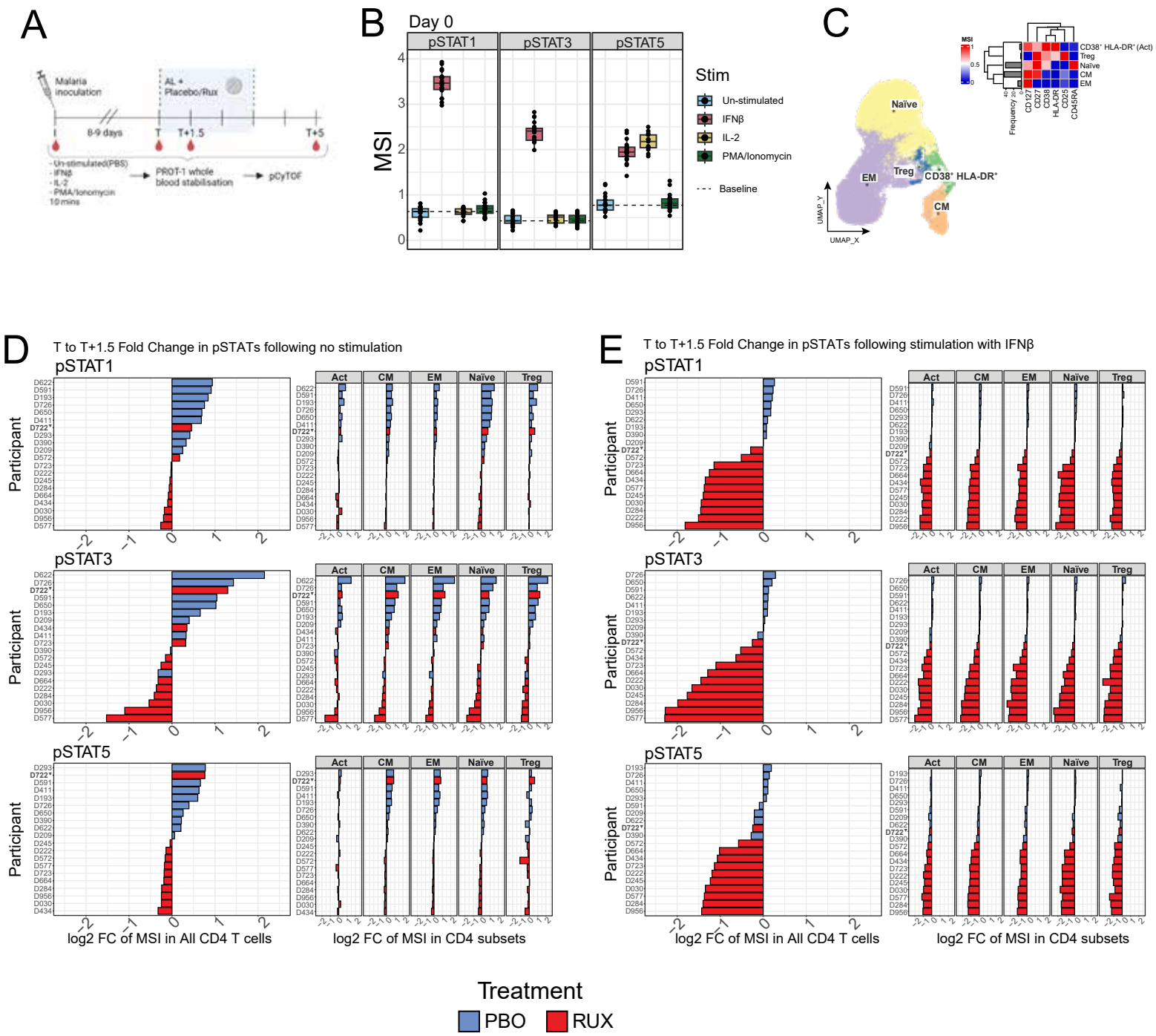

Figure 1: A. Ruxolitinib immune boosting study design and sample collection schedule for the whole blood phosphorylated protein assay. I indicates time of primary infection, T indicates treatment and the green box shows treatment period, which occurred twice daily for 3 days. **B.** Mean Signal Intensity (MSI) of phosphorylated STAT proteins in CD4+ T cells following stimulation of whole blood with PBS (un-stimulated condition), IFNβ, IL-2 and PMA/Ionomycin at the pre-inoculation (baseline) time point for 15 minutes. The box plots show the extent of the lower and upper quartiles and the median, while each point represents a study participant. **C.** UMAP visualisation of CD4+ T cell FlowSOM clustering showing 5 cell subsets identified using a heat map showing the expression of the CD4+ T cell markers. **D.** log 2 fold-change in the MSI of pSTAT1, pSTAT3 and pSTAT5 in all CD4+ T cells and CD4+ T cell subsets from pre-treatment (T) to treatment (T)+1.5 following no-stimulation. **E.** log 2 fold-change in the MSI of pSTAT1, pSTAT3 and pSTAT5 in all CD4+ T cells and CD4+ T cell subsets from pre-treatment (T) to treatment (T)+1.5 following stimulation of whole blood with IFNβ. Participant ▼D722 received only 2 doses of artemether/lumefantrine and ruxolitinib.

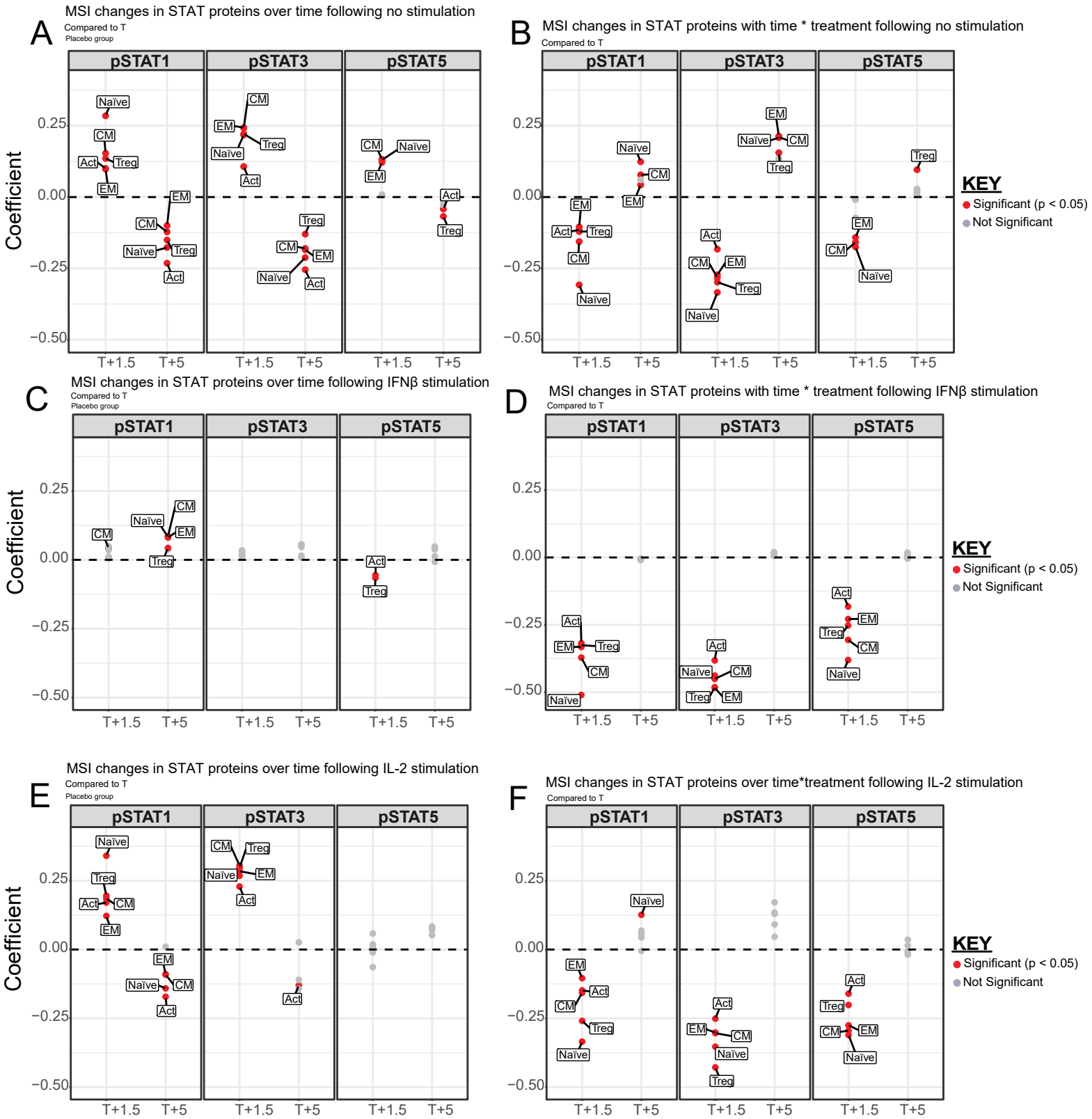

Figure 2: A. Plots showing the effect of time on the mean signal intensity (MSI) of the pSTAT proteins in CD4+ T cell subsets over the course of the first infection in the placebo group. **B.** Plots showing the effect of time and treatment on the MSI of the pSTAT proteins in CD4+ T cell subsets. **C.** Plots showing the effect of time on the MSI of the phosphorylated STAT (pSTAT) proteins in CD4+ T cell subsets following stimulation of whole blood with IFNβ during the treatment period of the first infection in the placebo group. **D**. Plots showing the effect of time and treatment on the MSI of the pSTAT proteins in CD4+ T cell subsets following stimulation of whole blood with IFNβ during the treatment period of the first infection. **E.** Plots showing the effect of time on the MSI of the phosphorylated STAT (pSTAT) proteins in CD4+ T cell subsets following stimulation of whole blood with IL-2 during the treatment period of the first infection in the placebo group. **F**. Plots showing the effect of time and treatment on the MSI of the pSTAT proteins in CD4+ T cell subsets following stimulation of whole blood with IL-2 during the treatment period of the first infection.

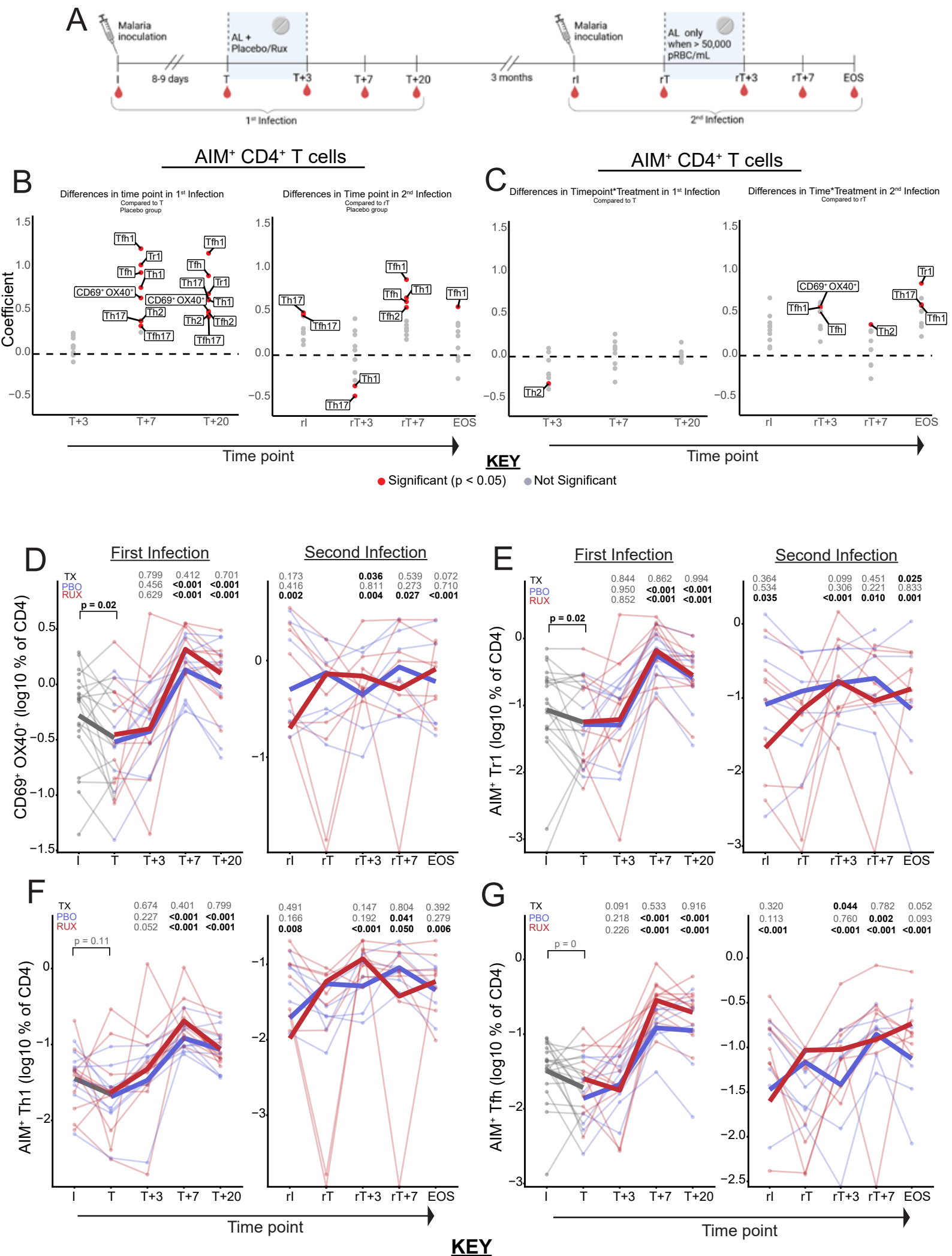
A
Malaria inoculation
AL + Placebo/Rux
8-9 days
I
T
T+3
T+7
T+20
1st Infection
3 months
Malaria inoculation
AL only when > 50,000 pRBC/mL
rI
rT
rT+3
rT+7
EOS
2nd Infection
B
AIM+ CD4+ T cells
Differences in time point in 1st Infection
Compared to T
Placebo group
Differences in Time point in 2nd Infection
Compared to rT
Placebo group
Coefficient
Time point
C
AIM+ CD4+ T cells
Differences in Timepoint*Treatment in 1st Infection
Compared to T
Differences in Time*Treatment in 2nd Infection
Compared to rT
Time point
KEY
Significant (p < 0.05)
Not Significant
D
First Infection
Second Infection
TX
PBO
RUX
p = 0.02
CD69+ OX40+ (log10 % of CD4)
E
First Infection
Second Infection
p = 0.02
AIM+ Tr1 (log10 % of CD4)
F
p = 0.11
AIM+ Th1 (log10 % of CD4)
Time point
G
p = 0
AIM+ Tfh (log10 % of CD4)
Time point
KEY
Placebo
Ruxolitinib
RUX - Rux Time point
PBO - Placebo Time point
TX - Treatment

Figure 3: Frequencies of antigen-specific $CD4^+$ T cells increase following anti-malariaL drug treatment. **A**. Blood draw schedule for the examination of peripheral blood mononuclear cells (PBMCs) from the CHMI participants for flow cytometry detection of activation-induced marker (AIM)-positive $CD4^+$ T cells. **B**. Plots showing the effect of time on the frequency of AIM^+ $CD4^+$ T cell subsets over the course of the first and second infection in the placebo group. **C**. Plots showing the effect of time and treatment on the frequency of AIM^+ $CD4^+$ T cell subsets over the course of the first and second infection. Linear mixed effects plots with prediction lines show *P. falciparum*-specific ($CD69^+$ $OX40^+$) **D**. $CD4^+$ T cells, **E**. Tr1 ($LAG3^+$ $CD49b^+$), **F**. Th1 ($CXCR5^-$ $CCR6^-$ $CCR4^-$ $CXCR3^+$)and **G**. Tfh ($CXCR5^+$ $PD1^+$) cell frequencies over the course of the first and second infection in the placebo (blue) and ruxolitinib (red) treated groups. PBMCs were acquired from the participants at time points indicated and re-stimulated with pRBCs for 18hrs, stained and acquired on the Cytek Aurora 5. Linear mixed effects model analysis was performed to determine the differences with time and treatment. The dots are representative of each AIM^+ $CD4^+$ T cell population measured as a frequency of total $CD4^+$ T cells. p values < 0.05 were considered significant. n = 20 for first infection (11 in the ruxolitinib group and 9 in the placebo group) and n = 14 for the second infection (8 in the ruxolitinib group and 6 in the placebo group). Due to limited cell samples, not all samples and/or time points from the study are shown in this figure.

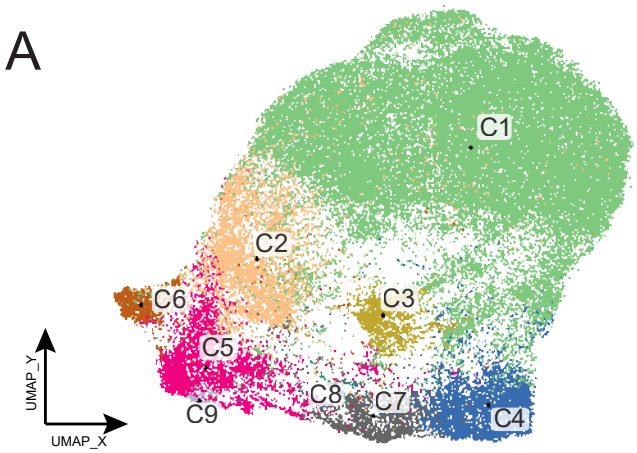
A
C1
C2
C3
C4
C5
C6
C7
C8
C9
UMAP_Y
UMAP_X

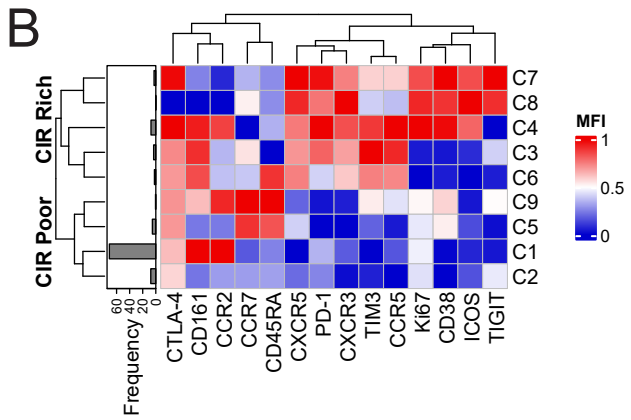
B
CIR Rich
CIR Poor
C7
C8
C4
C3
C6
C9
C5
C1
C2
MFI
1
0.5
0
Frequency
60
40
20
0
CTLA-4
CD161
CCR2
CCR7
CD45RA
CXCR5
PD-1
CXCR3
TIM3
CCR5
Ki67
CD38
ICOS
TIGIT

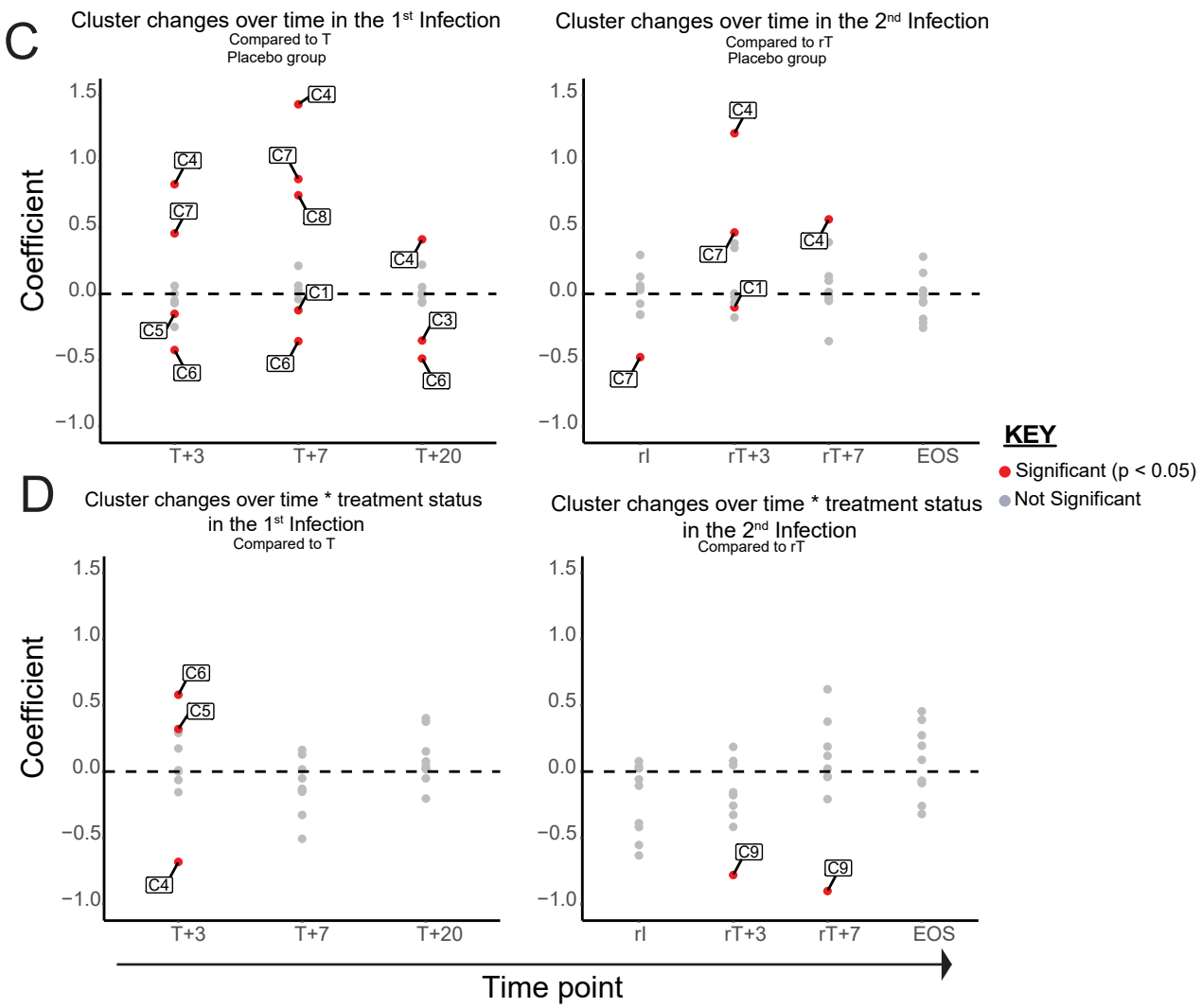
C
Cluster changes over time in the 1st Infection
Compared to T
Placebo group
Cluster changes over time in the 2nd Infection
Compared to rT
Placebo group
Coefficient
1.5
1.0
0.5
0.0
−0.5
−1.0
T+3
T+7
T+20
rI
rT+3
rT+7
EOS
KEY
Significant (p < 0.05)
Not Significant
D
Cluster changes over time * treatment status in the 1st Infection
Compared to T
Cluster changes over time * treatment status in the 2nd Infection
Compared to rT
Time point

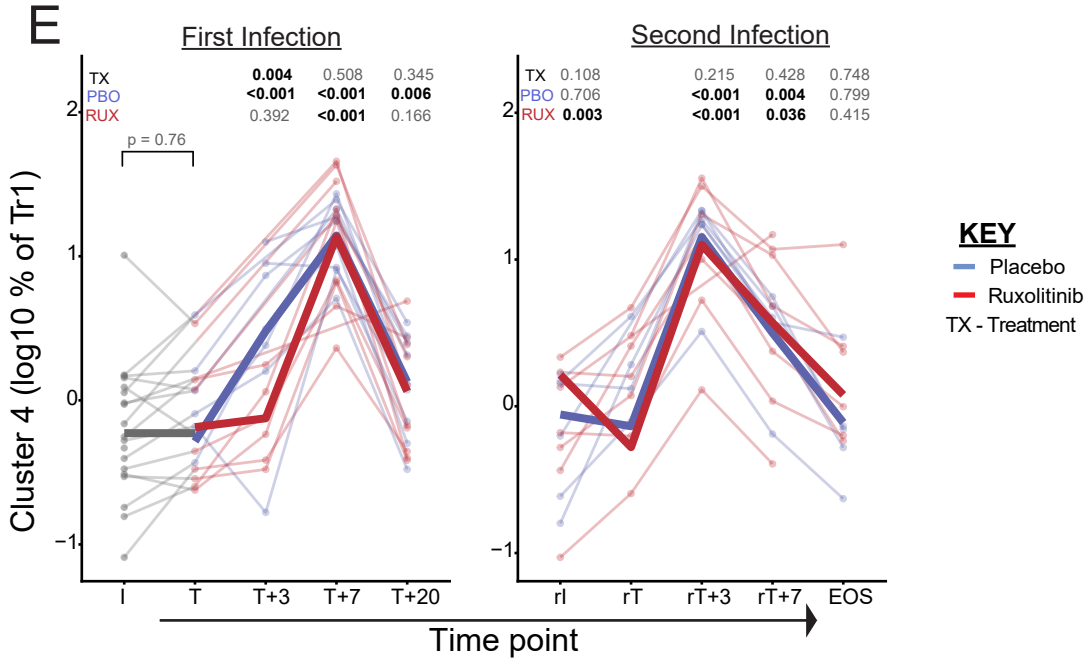
E
First Infection
Second Infection
TX 0.004 0.508 0.345
PBO <0.001 <0.001 0.006
RUX 0.392 <0.001 0.166
p = 0.76
TX 0.108 0.215 0.428 0.748
PBO 0.706 <0.001 0.004 0.799
RUX 0.003 <0.001 0.036 0.415
Cluster 4 (log10 % of Tr1)
2
1
0
−1
I
T
T+3
T+7
T+20
rI
rT
rT+3
rT+7
EOS
Time point
KEY
Placebo
Ruxolitinib
TX - Treatment

Figure 4: Increased frequencies of co-inhibitory receptor rich Tr1 clusters following anti-malarial drug treatment during the first and second infection. **A.** UMAP visualisation of Tr1 cell FlowSOM clustering showing the 9 clusters identified. **B.** Heat map showing the Tr1 cluster expression of co-inhibitory receptor markers and other markers of interest. **C.** Plots showing the effect of time on the frequency of the Tr1 clusters over the course of the first and second infection in the placebo group. **D.** Plots showing the effect of time and treatment on the frequency of Tr1 clusters over the course of the first and second infection. Linear mixed effects model analysis was performed to determine the differences in time and treatment. The dots are representative of a single Tr1 cell cluster. **E.** Predication line plots from the linear mixed effects model show the frequencies of co-inhibitory receptor rich cluster 4 as a percentage of total Tr1 cells in the first and second infection. The thin lines indicate the results from each individual and the bold dashed lines represent the average of the predicted values from each group obtained from linear mixed effects analysis where the fixed effects are the time point (TP) and treatment (TX) and the random effects are the individuals.p values $p < 0.05$ were considered significant. $n = 20$ for first infection (11 in the ruxolitinib group and 9 in the placebo group) and $n = 14$ for the second infection (8 in the ruxolitinib group and 6 in the placebo group). Flow cytometric analysis using Cytek Aurora 5 was carried on *ex vivo* PBMCs. Due to limited cell samples, not all samples and/or time points from the study were available for analysis in this experiment.

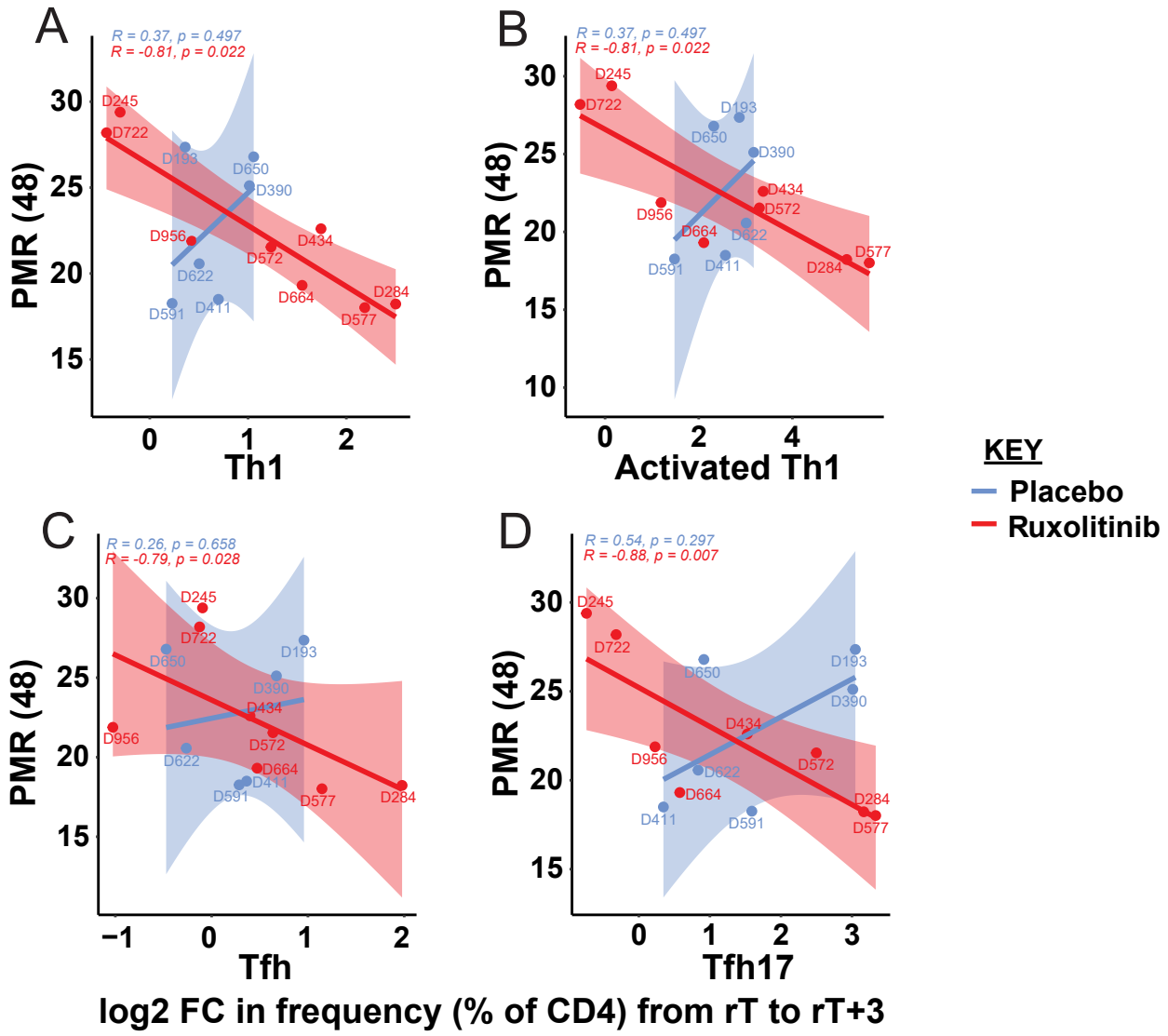

Figure 5: Correlation between the fold change in frequency of **A**. non-activated T helper 1 (Th1) cells ($CD4^+$ $CXCR3^+$ $CXCR5^-$), **B**. Activated ($CD38^+$ $HLA\text{-}DR^+$ $PD\text{-}1^+$ $ICOS^+$) Th1 cells, **C**. T follicular helper (Tfh) cells ($CD4^+$ $CXCR3^-$ $CXCR5^+$)and **D**. Tfh17 cells ($CD4^+$ $CXCR3^-$ $CXCR5^+$ $CCR6^+$), as a percentage of total CD4+ T cells from treatment (rT) to 3 days later (rT+3) during the second infection and the parasite multiplication rate per 48 hours (PMR48) following treatment with ruxolitinib (red) or placebo (blue) during the primary infection. n = 14 (8 in the ruxolitinib group, participant D722 included because they only received 2 doses and 6 in the placebo group). Each point represents a study participant. Statistics show Rho and p values calculated using the Spearman's correlations.

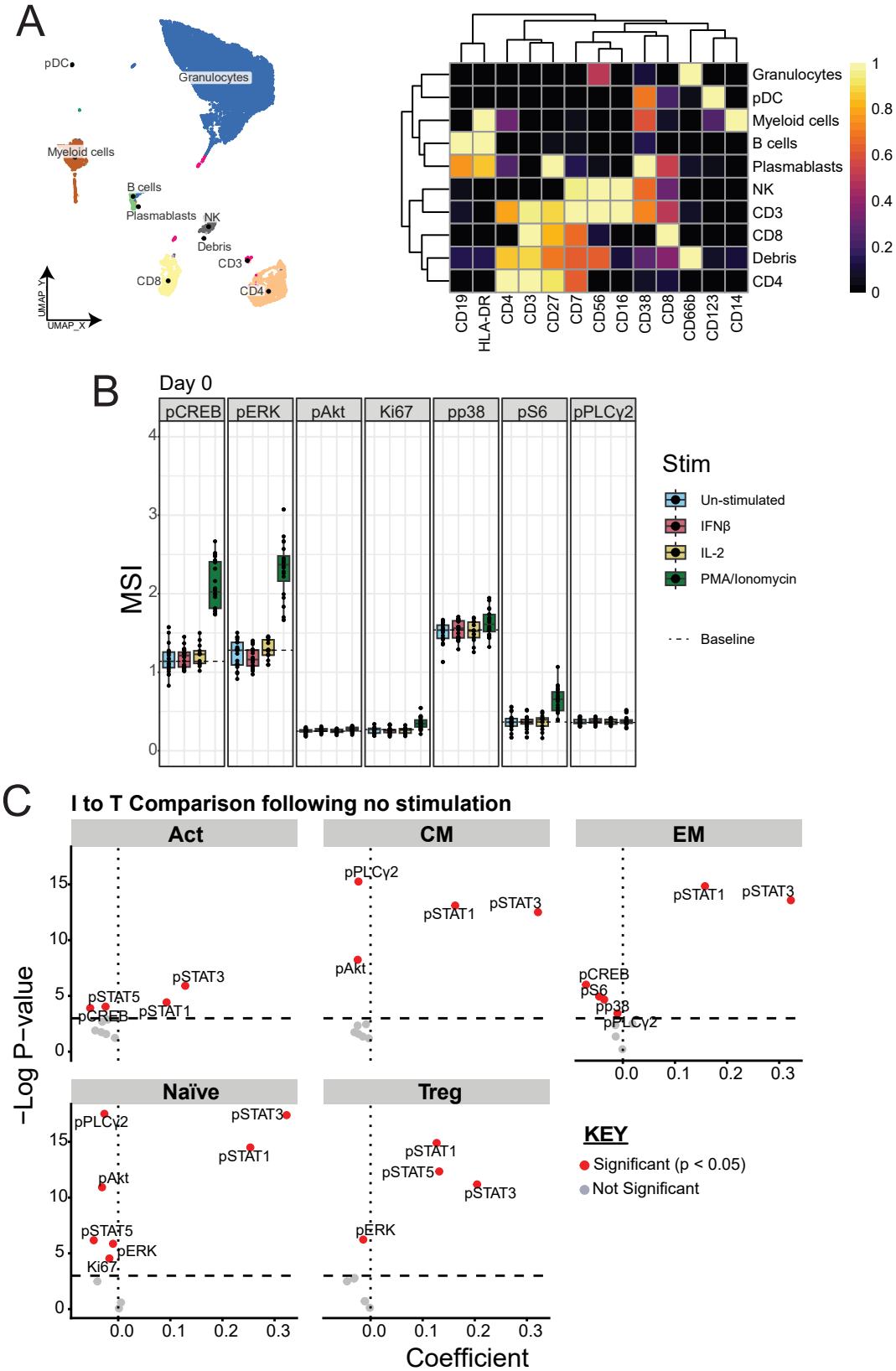

Supplementary Figure 1: **A.** UMAP clustering and heatmap of the whole blood cells used to identify immune cell subsets. **B.** Mean Signal Intensity (MSI) of phosphorylated proteins in CD4+ T cells following stimulation of whole blood with PBS (un-stimulated condition), IFNβ, IL-2 and PMA/Ionomycin at the pre-inoculation (baseline) time point for 15 minutes. The box plots show the extent of the lower and upper quartiles and the median, while each point represents a study participant. **C.** Volcano Plots showing the effect of infection on the mean signal intensity (MSI) of the phosphorylated proteins and Ki67 in CD4+ T cell subsets from the inoculation time point (I, day 0) to the pre-treatment time point (T, day 8/9).

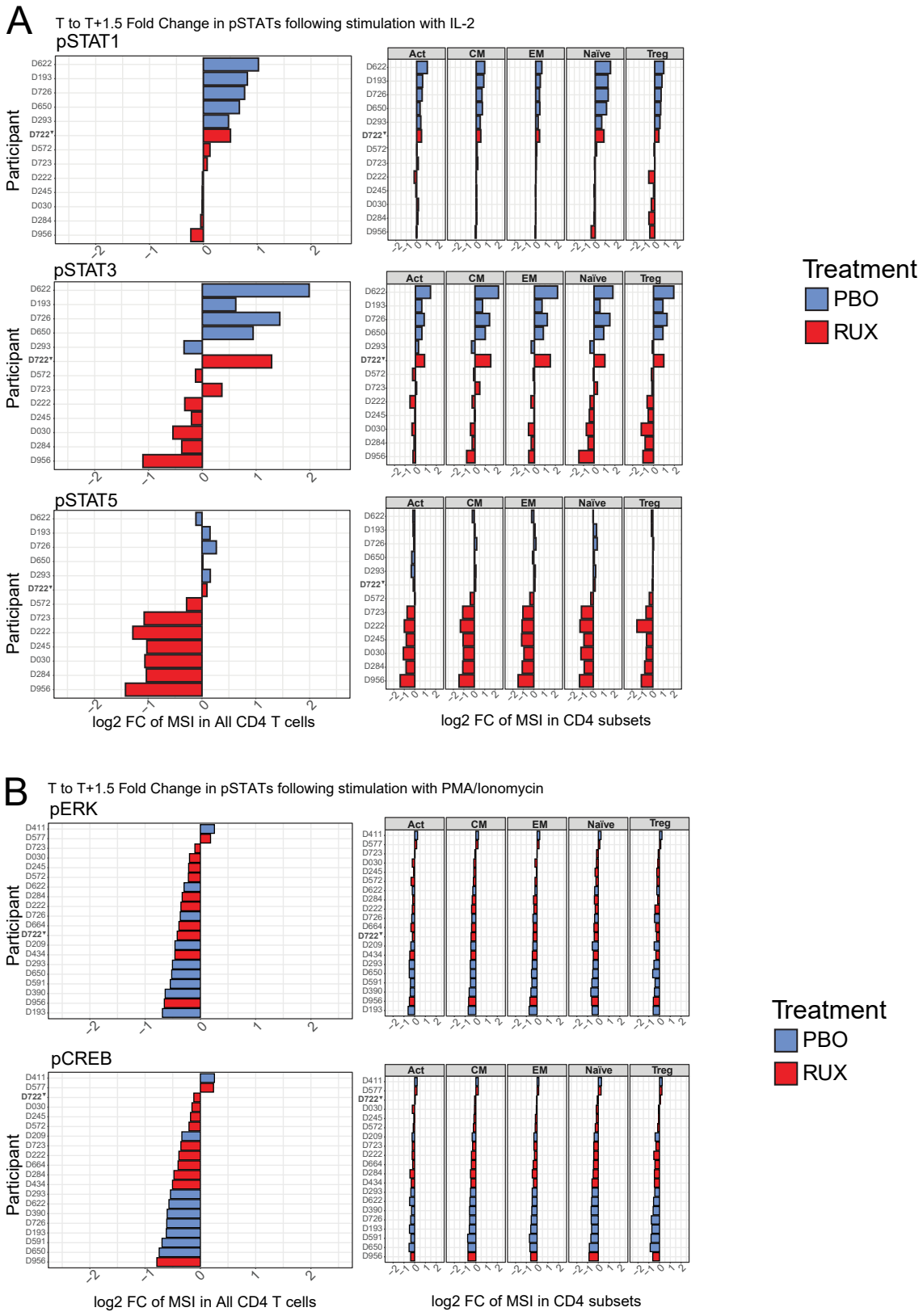

Supplementary Figure 2: **A.** log 2 fold-change in the MSI of pSTAT1, pSTAT3 and pSTAT5 in all CD4+ T cells and CD4+ T cell subsets from pre-treatment (T) to treatment (T)+1.5 following stimulation of whole blood with IL-2. Participant ▼D722 received 2 doses of ruxolitinib and arteer/lumefantrine. **B.** log 2 fold-change in the MSI of pERK and pCREB in all CD4+ T cells and CD4+ T cell subsets from pre-treatment (T) to treatment (T)+1.5 following stimulation of whole blood with PMA/Ionomycin. *Related to main Figure 1.*

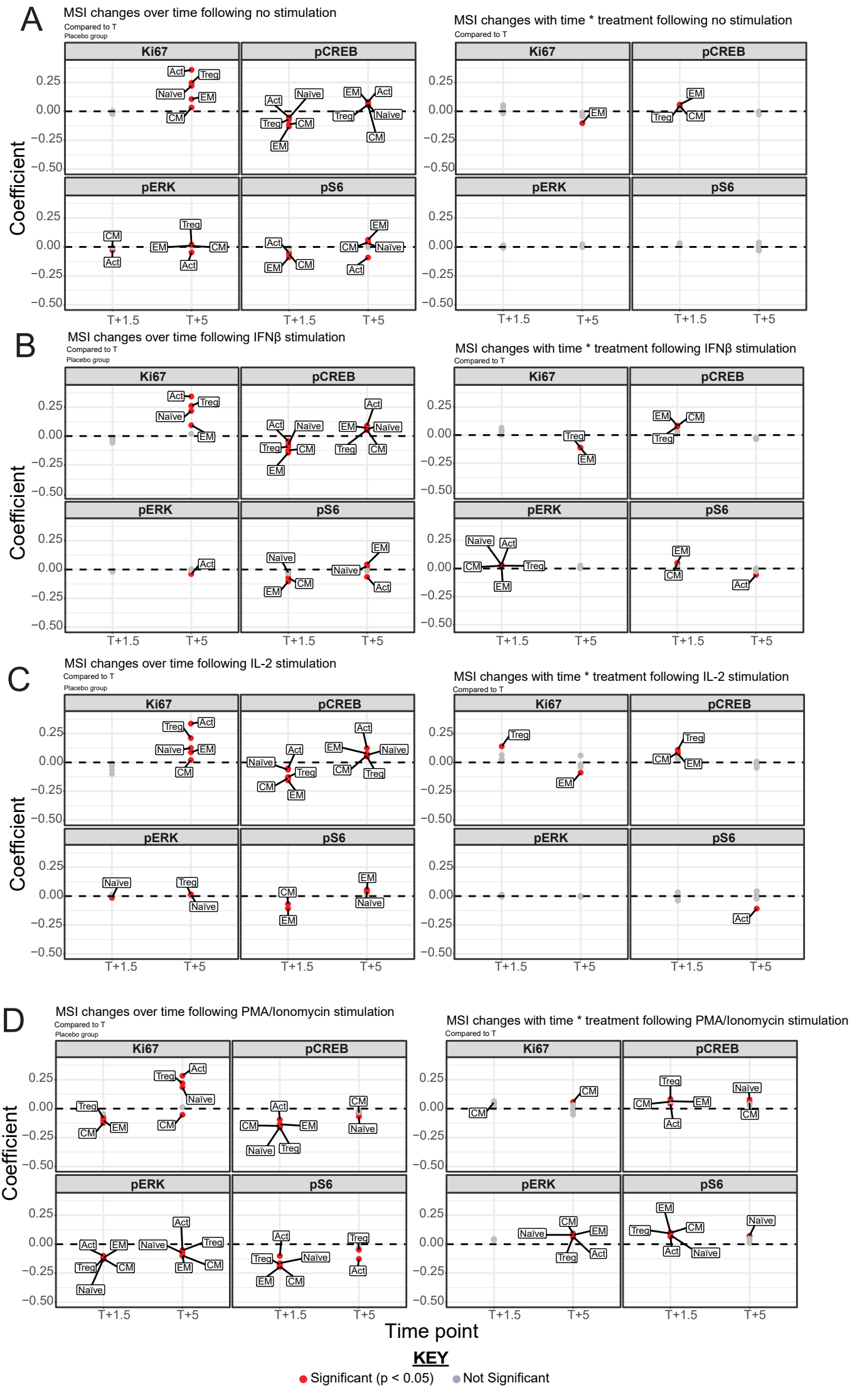
A
MSI changes over time following no stimulation
Compared to T
Placebo group
MSI changes with time * treatment following no stimulation
Compared to T
B
MSI changes over time following IFNβ stimulation
Compared to T
Placebo group
MSI changes with time * treatment following IFNβ stimulation
Compared to T
C
MSI changes over time following IL-2 stimulation
Compared to T
Placebo group
MSI changes with time * treatment following IL-2 stimulation
Compared to T
D
MSI changes over time following PMA/Ionomycin stimulation
Compared to T
Placebo group
MSI changes with time * treatment following PMA/Ionomycin stimulation
Compared to T
Ki67
pCREB
pERK
pS6
Coefficient
0.25
0.00
−0.25
−0.50
T+1.5
T+5
Time point
KEY
Significant (p < 0.05)
Not Significant

Supplementary Figure 3: Plots showing the effect of time and the effect of time and treatment on the on the mean signal intensity (MSI) of the phosphorylated proteins and Ki67 in CD4+ T cell subsets over the course of the first infection in the placebo group following .**A.** no stimulation and stimulation with **B.** IFNβ, **C.** IL-2 and **D.** PMA/Ionomycin. *Related to main Figure 2.*

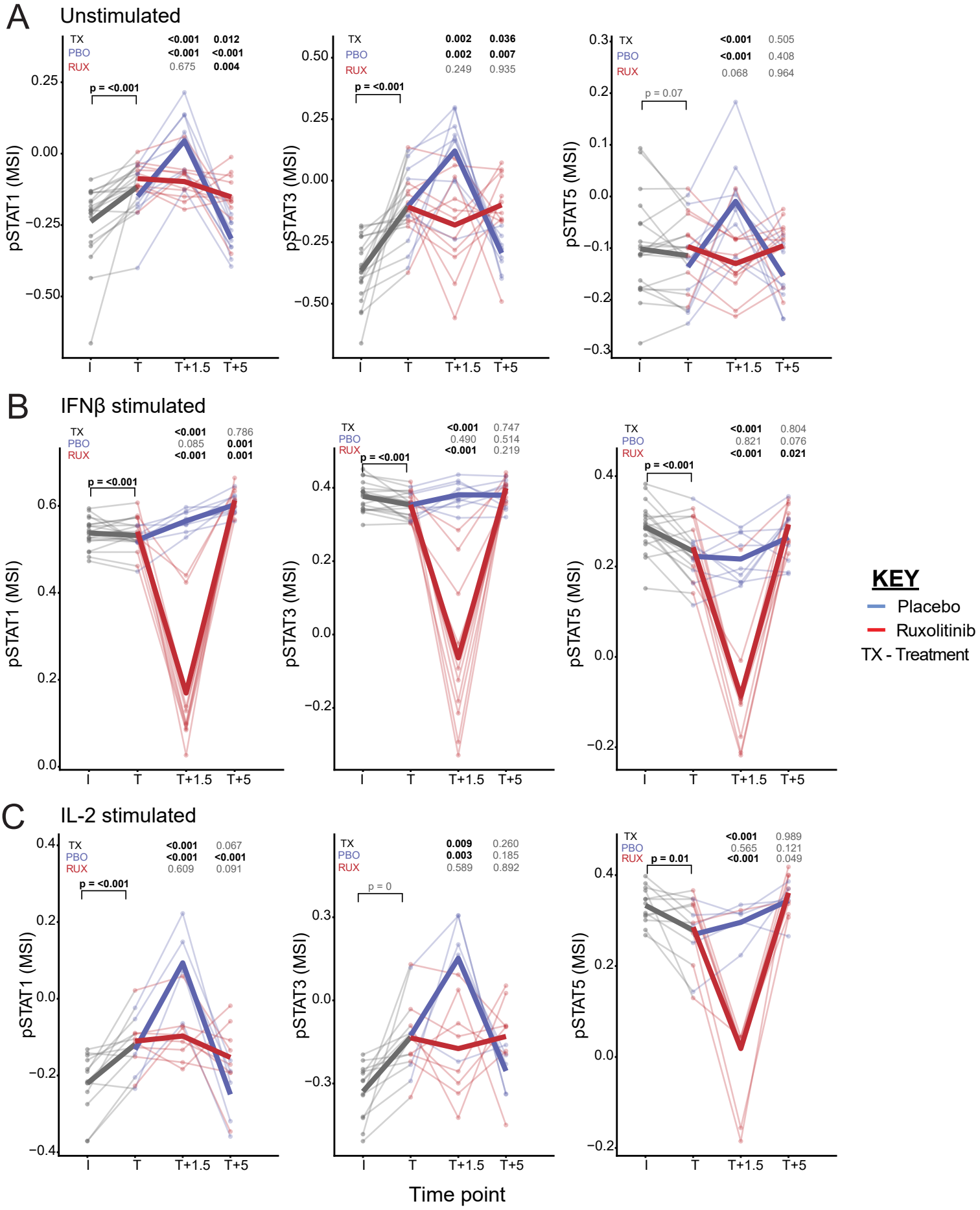

Supplementary Figure 4: Plots showing the effect of time and treatment on the MSI of the pSTAT1, 3 and 5 proteins in all CD4+ T cells following **A**. no stimulation, **B.** stimulation with IFN β and C. stimulation with IL-2. The thin lines indicate the results from each individual and the bold dashed lines represent the predicted average from each group obtained from linear mixed effects model analysis where the fixed effects are the time point in each of the treatment conditions (RUX and PBO) and treatment (TX) and the random effects are the individuals. The grey ribbon indicates the lower and upper spread of the mean of the predicted values. p values were $p < 0.05$. ns = not significant ($p > 0.05$). n = 20 (11 in the ruxolitinib group and 9 in the placebo group) for the unstimulated and IFNβ condition. n = 13 (8 in the ruxolitinib group and 5 in the placebo group) for the IL-2 condition.
Related to main Figure 2.

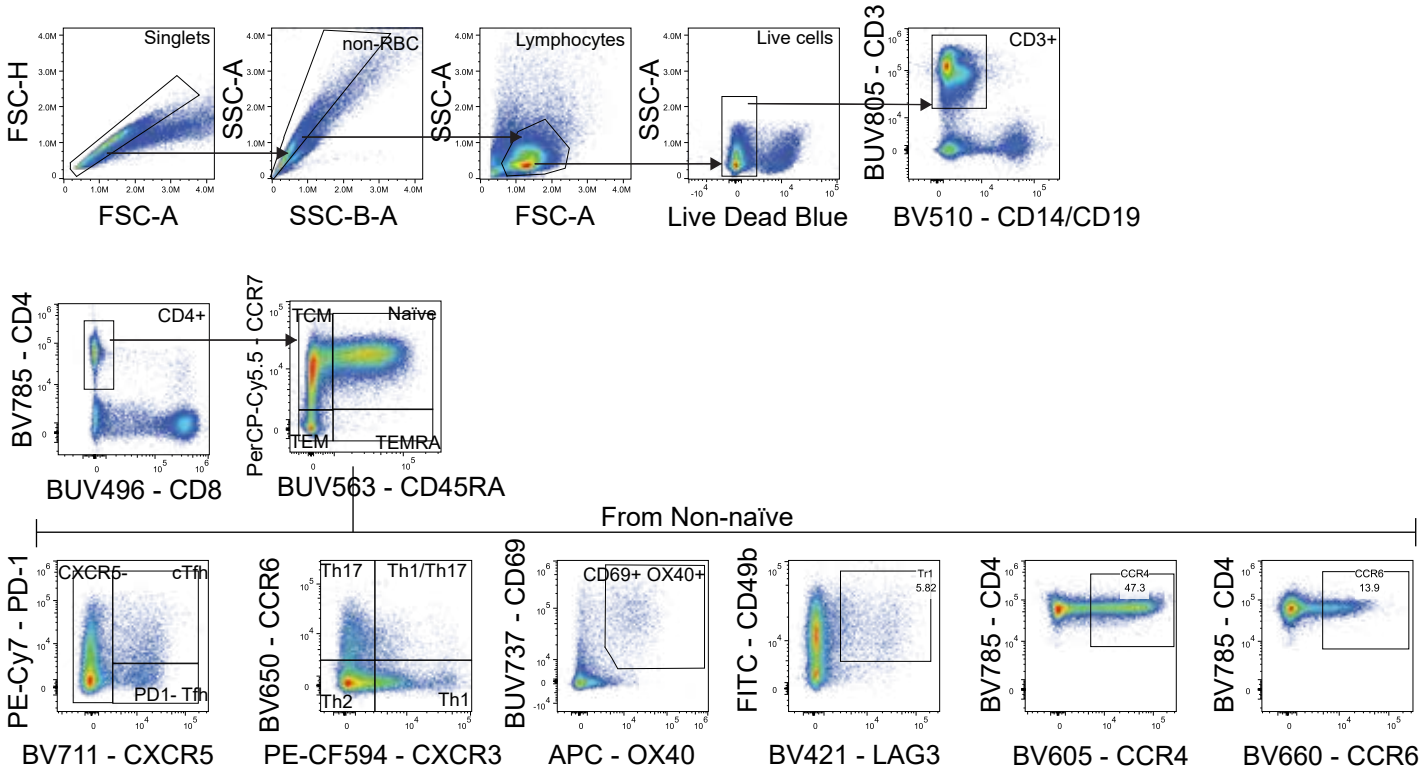

Supplementary Figure 5: Gating Strategy employed to identify the AIM+ CD4+ T cell populations in FlowJo. After gating for the CD45RA+ CCR7+ naive cells, a "not" gate was used to remove this population and the other CD4+ T cell subsets were identified from the non-naive CD4+ T cells. Following this, boolean gating was using to examine AIM+ CD4+ T cells. Figure represents PBMCs from Day 15 for D726 in the Placebo group following 18 hour culture with parasitised red blood cells.
Related to main Figure 3.

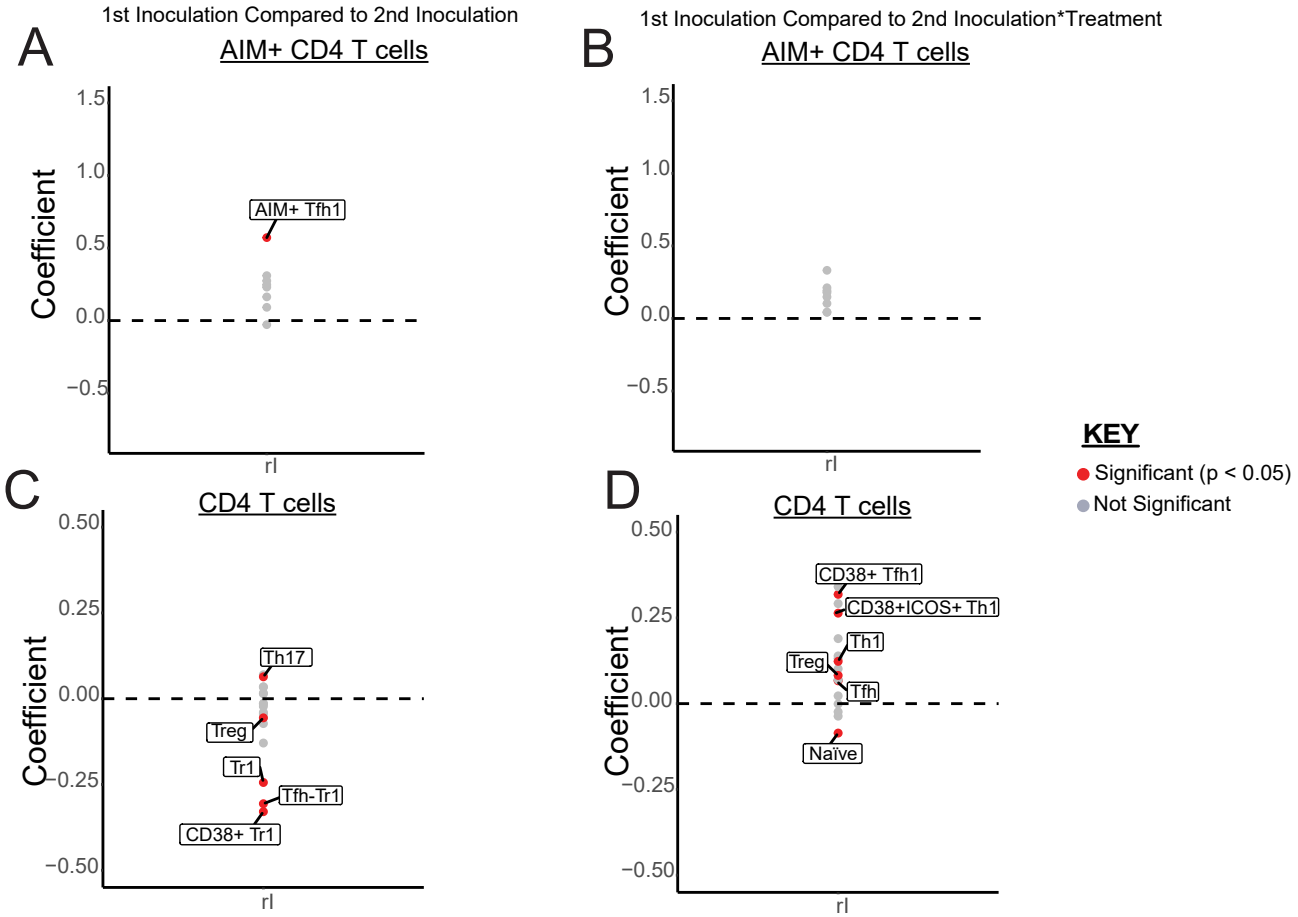

Supplementary Figure 6: Dot plots showing the effect of **A**. time and **B**. the effect of time point and treatment on the frequencies of the AIM+ CD4+ T cell subsets comparing the 1st inoculation time point (I) to the re-inoculation time point (rI) as assessed by flow cytometry. Dot plots showing the effect of **C**. time and **D**. the effect of time point and treatment on the frequencies of the CD4+ T cell subsets comparing the 1st inoculation time point (I) to the re-inoculation time point (rI) as asssessed by mass cytometry.
Related to main Figure 3 and Supplementary Figure 5 .

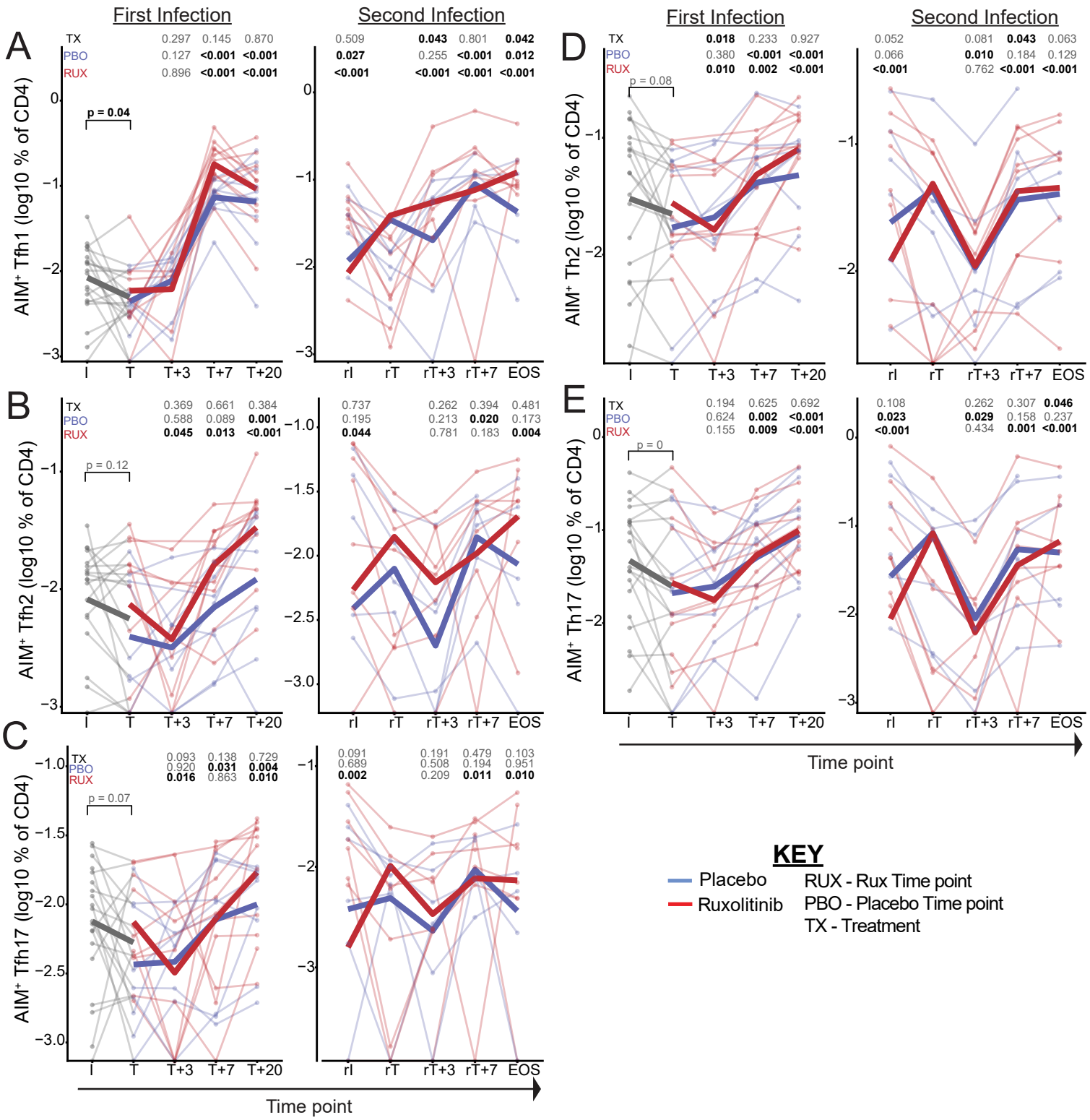

Supplementary Figure 7: Linear mixed effects plots with prediction lines show *P. falciparum*-specific (CD69$^+$ OX40$^+$) **A**. Tfh1 cells, **B**. Tfh2, **C**. Tfh17 , **D**. Th2 and **E.** Th17 cell frequencies over the course of the first and second infection in the placebo (blue) and ruxolitinib (red) treated groups. PBMCs were acquired from the participants at time points indicated and re-stimulated with pRBCs for 18hrs, stained and acquired on the Cytek Aurora 5. Linear mixed effects model analysis was performed to determine the differences with time and treatment. The dots are representative of each AIM$^+$ CD4$^+$ T cell population measured as a frequency of total CD4$^+$ T cells. p values < 0.05 were considered significant. n = 20 for first infection (11 in the ruxolitinib group and 9 in the placebo group) and n = 14 for the second infection (8 in the ruxolitinib group and 6 in the placebo group). Due to limited cell samples, not all samples and/or time points from the study are shown in this figure.
Related to main Figure 3.

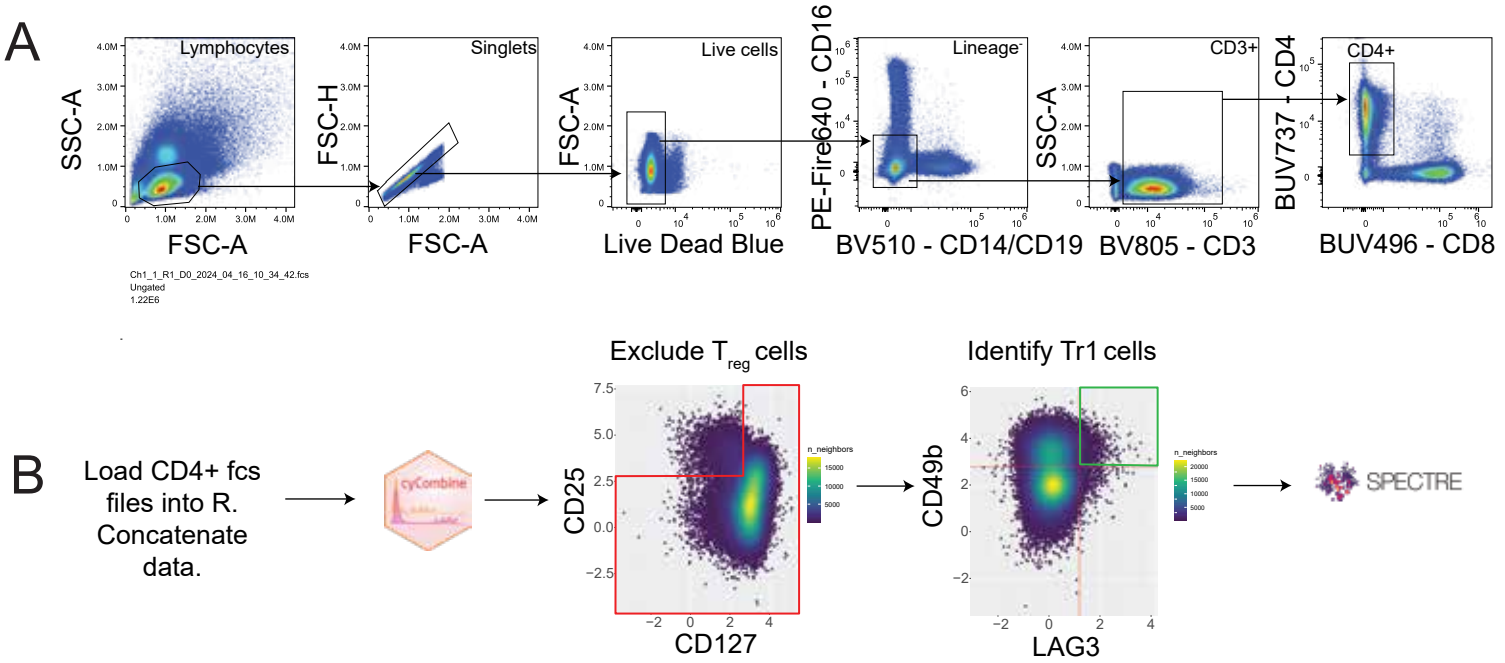

Supplementary Figure 8: Gating Strategy employed to identify the type I regulatory CD4+ T cells in the ruxolitinib immune boosting clinical trial. a. After flow cytometry, CD4+ T cells were identified in FlowJo and the 3.0 fcs files were exported. b. Following this, the files were concatenated and batch correction was performed using cyCombine. Treg cells were excluded from the CD4+ T cell population and the Tr1 cells identified using LAG3 and CD49b. Downstream analysis of the Tr1 cells was carried out in Spectre. *Related to main Figure 4.*

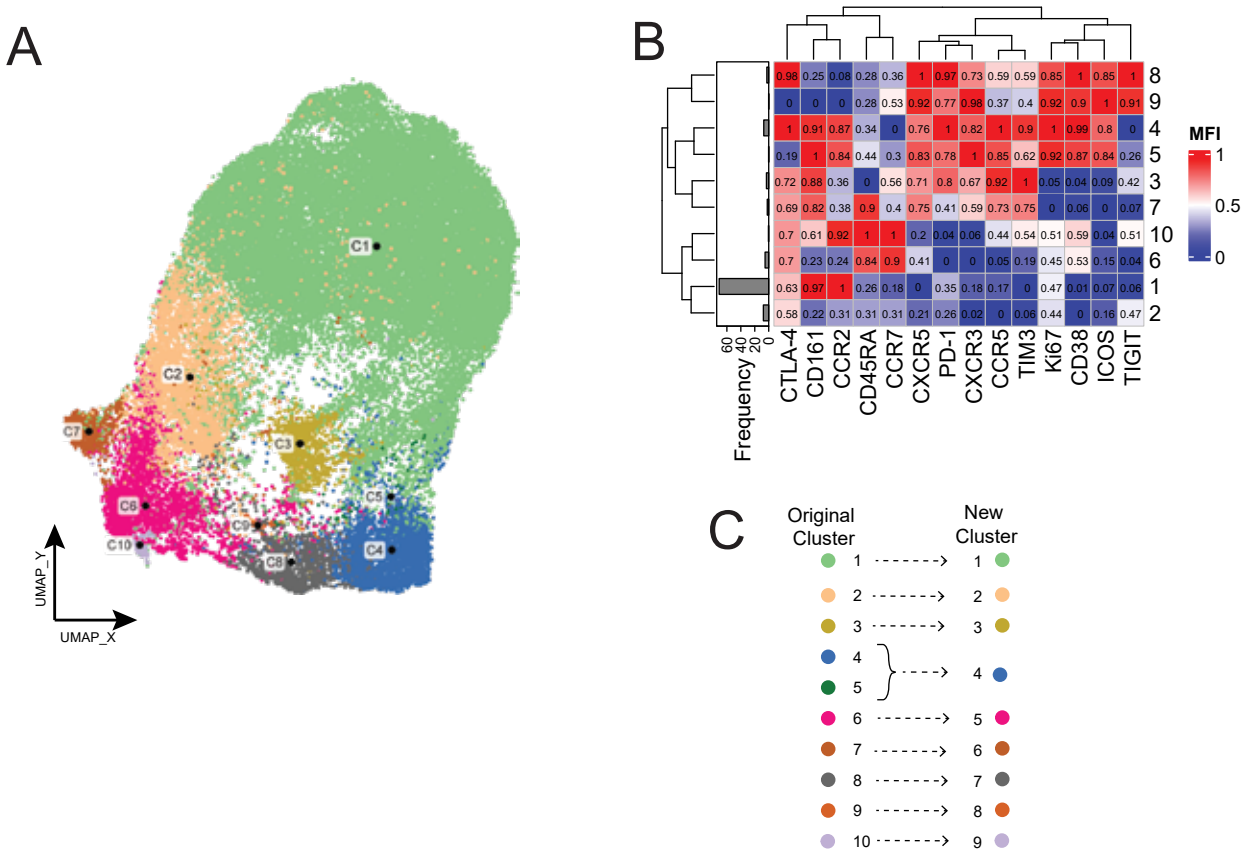

Supplementary Figure 9:**A.** Tr1 cell UMAP showing the 10 different clusters. B. Cluster 4 and 5 have similar expression of co-inhibitory markers, with only CTLA-4 differing between the two. Co-inhibitory receptor rich clusters were defined as clusters with > 0.5 expression of at least 4 co-inhibitory markers, otherwise, they were defined as co-inhibitory receptor poor. **C.** Combination of the co-inibitory receptor rich cluster 4 and 5 into a single cluster named cluster 4. The other clusters were then renamed. *Related to main Figure 4.*

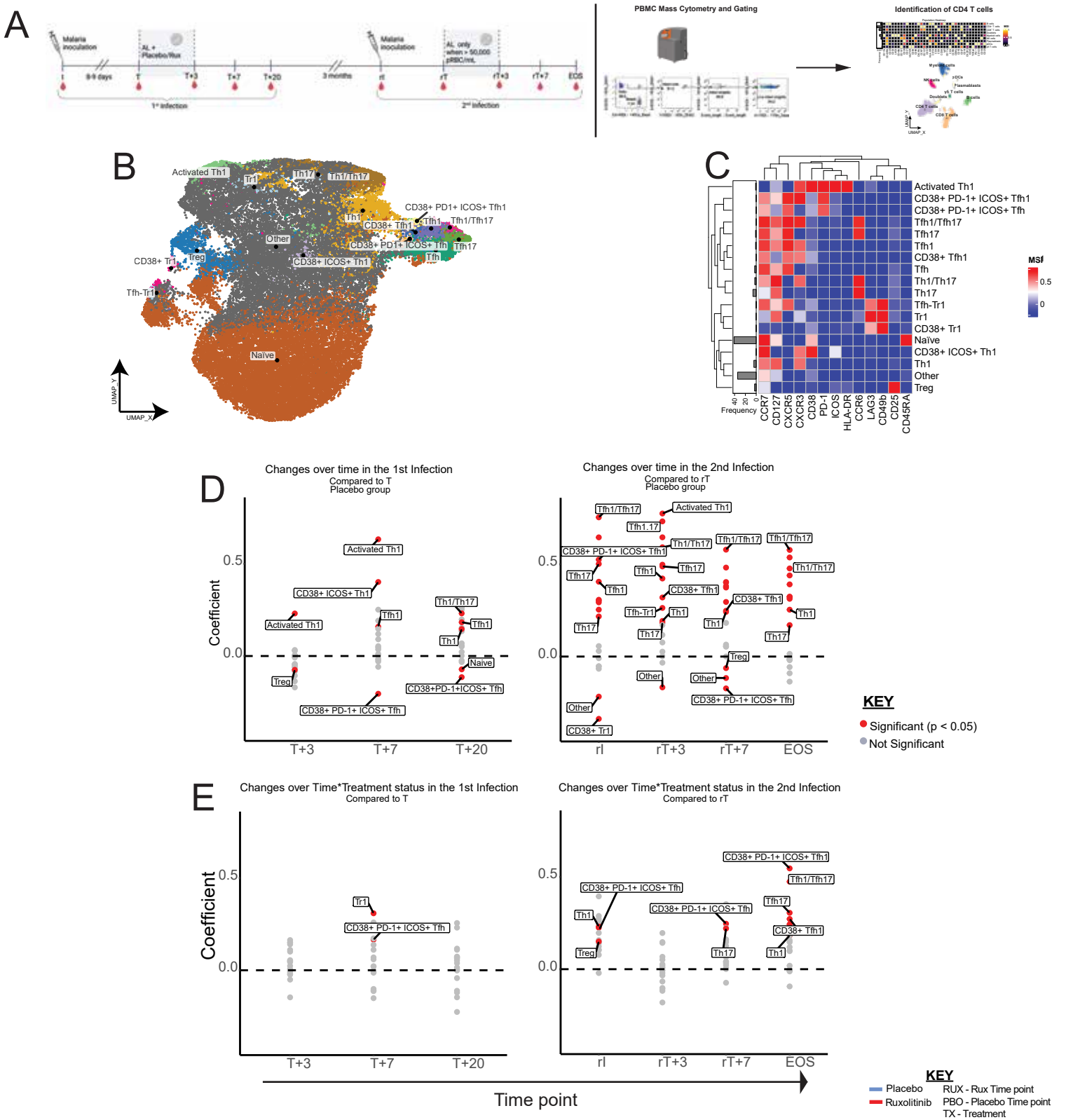
A
Malaria inoculation
AL + Placebo/Rux
8-9 days
I
T
T+3
T+7
T+20
1st infection
3 months
Malaria inoculation
AL only when > 50,000 pRBC/mL
rI
rT
rT+3
rT+7
EOS
2nd infection
PBMC Mass Cytometry and Gating
Identification of CD4 T cells
B
Activated Th1
Tr1
Th17
Th1/Th17
CD38+ PD1+ ICOS+ Tfh1
Th1
CD38+ Tfh1
Tfh1
Tfh1/Tfh17
Other
CD38+ PD1+ ICOS+ Tfh
Tfh17
Tfh
CD38+ Tr1
Treg
CD38+ ICOS+ Th1
Tfh-Tr1
Naïve
UMAP_Y
UMAP_X
C
Activated Th1
CD38+ PD-1+ ICOS+ Tfh1
CD38+ PD-1+ ICOS+ Tfh
Tfh1/Tfh17
Tfh17
Tfh1
CD38+ Tfh1
Tfh
Th1/Th17
Th17
Tfh-Tr1
Tr1
CD38+ Tr1
Naïve
CD38+ ICOS+ Th1
Th1
Other
Treg
MSI
0.5
0
Frequency
40
20
0
CCR7
CD127
CXCR5
CXCR3
CD38
PD-1
ICOS
HLA-DR
CCR6
LAG3
CD49b
CD25
CD45RA
D
Changes over time in the 1st Infection
Compared to T
Placebo group
Coefficient
0.5
0.0
T+3
T+7
T+20
Activated Th1
CD38+ ICOS+ Th1
Tfh1
Activated Th1
Th1/Th17
Tfh1
Th1
Naïve
Treg
CD38+PD-1+ICOS+ Tfh
CD38+ PD-1+ ICOS+ Tfh
Changes over time in the 2nd Infection
Compared to rT
Placebo group
rI
rT+3
rT+7
EOS
Tfh1/Tfh17
Activated Th1
Tfh1.17
Th1/Th17
Tfh1/Tfh17
Tfh1/Tfh17
CD38+ PD-1+ ICOS+ Tfh1
Tfh17
Tfh1
Tfh17
Th1/Th17
Tfh17
Tfh1
CD38+ Tfh1
CD38+ Tfh1
Tfh-Tr1
Th1
Th1
Th1
Th17
Th17
Th17
Treg
Other
Other
CD38+ PD-1+ ICOS+ Tfh
Other
CD38+ Tr1
KEY
Significant (p < 0.05)
Not Significant
E
Changes over Time*Treatment status in the 1st Infection
Compared to T
Coefficient
0.5
0.0
T+3
T+7
T+20
Tr1
CD38+ PD-1+ ICOS+ Tfh
Changes over Time*Treatment status in the 2nd Infection
Compared to rT
rI
rT+3
rT+7
EOS
CD38+ PD-1+ ICOS+ Tfh1
Tfh1/Tfh17
CD38+ PD-1+ ICOS+ Tfh
Tfh17
Th1
CD38+ PD-1+ ICOS+ Tfh
CD38+ Tfh1
Treg
Th17
Th1
Time point
KEY
Placebo
Ruxolitinib
RUX - Rux Time point
PBO - Placebo Time point
TX - Treatment
F
First Infection
Second Infection
TX
PBO
RUX
0.714 0.010 0.066
0.999 <0.001 0.015
0.584 0.377 0.943
0.026 0.150 0.014 0.019
0.391 0.982 0.023 0.089
0.017 0.023 0.269 0.101
p = 0.34
CD38+ PD-1+ ICOS+ Tfh (log10 % of CD4)
−0.5
−1.0
−1.5
−2.0
−0.4
−0.8
−1.2
−1.6
I
T
T+3
T+7
T+20
rI
rT
rT+3
rT+7
EOS
Time point
G
First Infection
Second Infection
TX
PBO
RUX
0.348 0.090 0.478
0.046 <0.001 0.088
0.429 <0.001 0.003
0.469 0.975 0.669 0.567
0.022 <0.001 0.003 0.017
<0.001 <0.001 <0.001 <0.001
p = <0.001
Activated Th1 (log10 % of CD4)
1.0
0.5
0.0
−0.5
−1.0
I
T
T+3
T+7
T+20
rI
rT
rT+3
rT+7
EOS
Time point

Supplementary Figure 10: **A**. Clinical study design and analytical pipeline for the mass cytometry analysis of PBMCs from participants in the ruxolitinib immune boosting study. Following gating for live intact signlet cells in FlowJo, immune cell subsets were identified using FlowSOM clustering in Spectre with a k value of 15 and annotated according to their expression of cell lineasge markers as shown in the heat map **B.** UMAP visualisation of CD4+ T cell FlowSOM clustering showing the 18 cell subsets identified. **C.** Heat map showing the CD4+ T cell subset expression of associated chemokine and activation markers. Linear mixed effects analysis was performed to determine the differences in time and treatment. Plots showing the effect of time on the frequency of CD4+ T cell subsets over the course of the **D.** first and second infection in comparison to the respective treatment time points in each phase. **E.** Plots showing the effect of time and treatment on the frequency of CD4+ T cell subsets over the course of the first and second infection in comparison to the respective treatment time points in each phase.Linear mixed effects plots with prediction lines show **F.** CD38+ PD-1+ ICOS+ Tfh cells and **G.** Activated (CD38+ PD-1+ ICOS+ HLA-DR+) cell frequencies over the course of the first and second infection in the placebo (blue) and ruxolitinib (red) treated groups. The points are representative of each $CD4^+$ T cell population measured as a frequency of total $CD4^+$ T cells. p values < 0.05 were considered significant. n = 20 for first infection (11 in the ruxolitinib group and 9 in the placebo group) and n = 14 for the second infection (8 in the ruxolitinib group and 6 in the placebo group).